COMBINATORIAL TARGETED THERAPIES

FOR THE TREATMENT OF

GLIOBLASTOMA TUMORSPHERE LINES

A Dissertation

Presented to the Faculty of the Weill Cornell Graduate School

of Medical Sciences

in Partial Fulfillment of the Requirements for the Degree of

Doctor of Philosophy

by

Poorvi Kaushik

February 2016

COMBINATORIAL TARGETED THERAPIES FOR THE TREATMENT OF GLIOBLASTOMA TUMORSPHERE LINES

Poorvi J. Kaushik, PhD.

Cornell University 2016

The depth of our knowledge about the molecular genetics of glioblastoma (GBM) stands in stark contrast with our ability to treat it successfully. This work reports research aimed at developing combination therapies to effectively inhibit cell growth in GBM tumorspheres. In our first study, our goal was to identify synergistic pairs of drugs across three tumorsphere lines bearing genomic alterations representative of the established signaling subclasses of GBM tumors – the NF1 deleted (represented by the tumorsphere line TS565), PGDFRA amplified (represented by the tumorsphere line TS543) and EGFR activated (represented by the tumorsphere line TS676) types. Using 12 targeted drug pairs, we identified drug combinations whose effects were cell-line specific and reduced cell viability compared to the single drugs. We quantified synergy using two measures, the well known Combination Index, as well as a measure we defined as the Efficacy Index that is able to detect synergies in instances where the Combination Index defined at 50% is unable to capture synergy. Predominant among the synergistic drug combinations we report are the combination of MEK and AKT1/2 inhibition in the line TS543, that of the drugs gefitinib (EGFRi) and AG538 (IGFRi) in line TS565 and of gefitinib and stattic (STAT3i) in line TS676.

In a second study, we sought to extend our findings from combination therapies to a clinically distinct, frequently observed subset of treatment resistant EGFR-driven GBM tumors. To improve the efficacy of EGFR inhibition, we rationally selected drugs that that may synergize with lapatinib based on the action of their

respective targets on key oncogenic pathways, and explored the optimal sequence and timing of administration. In TS676 tumorspheres, which have an EGFR amplification, express the EGFRvIII mutantation and have low PTEN expression, the combination of lapatinib and obatoclax was synergistic when obatoclax was applied before lapatinib. The observed synergy correlated positively with time delays from 3h to 24h. We then studied this combination in two other tumorsphere lines TS600, with an EGFR gain, and GBM39, which is EGFR amplified with the vIII mutation but PTEN intact. Sequential administration was only mildly beneficial in TS600 and not beneficial in GBM39. A time-course protein array experiment designed to illuminate the network aspects of the effects of lapatinib and obatoclax in TS676 and TS600 revealed that the most effective sequential combination in TS676 was obatoclax preceding lapatinib by 12h. This was associated with higher cleaved caspase-3 activation than the less effective co-treatment with lapatinib and obatoclax. We applied network based modeling methodologies to help test hypotheses that may explain the increased vulnerability of TS676 to lapatinib upon pretreatment with obatoclax.

This study presents encouraging results demonstrating the role of drug combination timing and order on the observed effect and synergy of therapies aimed at treating EGFR driven GBM tumorspheres. We show that BCL2 inhibition by obatoclax offers a potent and promising means of increasing cellular sensitivity to lapatinib. However, further work in other EGFR driven GBM models that have lost PTEN expression is a desirable next step towards revealing the relationship of sequential synergy to this well studied co-occurrence of genetic alterations.

BIOGRAPHICAL SKETCH

My life so far has been marked by an agreeable combination of privilege and perspective. At many turns I have been lucky enough to advance to where I wanted to be next, but my experience has been peppered with just enough adversity that I recognize my privilege. I grew up in Saudi Arabia, which meant that I got to watch Sesame Street while I also became comfortable with the idea of the burqa and not being able to play outdoors. My mother, who is among the most intelligent and empathic people I have known, became a house-wife when she moved with her family to Saudi Arabia, and adjusted the expectations she had of life to match the possibilities presented to her. My desire to make up for the time and experiences she lost became a big driver of my own ambition and scientific curiosity.

My interest in science also stems from my desire for authenticity in how I touch and am touched by life. While my years in graduate school have begun to help me learn the scientific method, I realize more clearly every day how variegated its paths are. This makes me very excited for my future and all that remains to be discovered and experienced. I am hopeful that the tools I am gathering will allow me to do work that serves my own happiness and that of the less privileged among us.

AKCNOWLEDGEMENTS

I am deeply indebted to my adviser Chris Sander for the opportunity to work in his lab. I was interested in science in an abstract way before I joined the lab, and the support and opportunities he gave to me in my years of exploration and discovery and during my setbacks have been instrumental to my success. Chris has a way of cutting through the noise in a problem and seeing what is important. This trait of his has been just as useful to me when he was critiquing some of my experimental results, as it was when I felt afraid or unsure of myself.

I am equally grateful to my co-adviser, the neurosurgeon Cameron Brennan, whose work treating patients with glioblastoma originally motivated this research. His knowledge and support are the reason I am putting these words to paper today. Our numerous meetings and his perspectives on my work at every level have helped shape my thinking in important and lasting ways and I hope that I am able some day to emulate his unique combination of scientific insight and compassion.

I am greatly indebted to David Christini for selecting me into the Tri-I CBM program. It has been the best opportunity of my life. I also wish to thank the members of my committee, Ingo Mellinghoff, Joao Xavier, and Jeffrey Varner for their support as well as all in the Sander and Brennan lab who have supported me in my work and life here. Debra Bemis provided essential managerial support, helping us to organize the processes and plans that our work involved, while also contributing her valuable scientific expertise at critical times in the progress of this work. Rita Gangi-Dino made the process of finishing this thesis as pleasant and stress-free as possible, and her moral support at all times has been invaluable. I would like to thank Evan Molinelli and Phaedra Agius for their friendship, brain-

TABLE OF CONTENTS

LIST OF TABLES

LIST OF FIGURES

CHAPTER 1
INTRODUCTION

Among the most thoroughly profiled cancers to date, primary glioblastoma (GBM) is a tumor of the brain that is characterized by heterogeneity, invasiveness and a profound lack of response to targeted treatment. Studies that began in the early 2000s by the work of groups including The Cancer Genome Atlas (TCGA) revealed the existence of transcriptomally defined subtypes within GBM designated as proneural, mesenchymal, neural, and classical [1-3] and recurrent mutations in the canonical signaling pathways that drive these tumors [4]. The GBM research community has made useful predictive and therapeutic recommendations in small subsets of patients [5, 6] and the molecular drivers of resistance are actively being studied in preclinical and clinical settings [7-10]. However, the majority of efforts to therapeutically target recurrent mutations in GBM have failed to show survival benefit in patients. Consequently, two broad questions pertaining to GBM therapy have been why drugs that target these known alterations have been ineffective, and whether there exist molecular markers that can reliably predict patient response to treatment.

Lack of treatment response in GBM is the result of many interacting phenomena, some of which we have begun to understand. For one, GBM's location in the brain makes it challenging for any systemically administered therapeutic to cross the blood brain barrier (BBB). Efflux transporters located at the BBB can rapidly quench the tissue of drug, and many agents that enter clinical trials actually bind to these efflux transporters with high affinity [11, 12]. Consequently, there is of-

ten not enough drug in the tissue, and when there is, it can be shunted out quickly.

In addition, the considerable inter- and intratumoral heterogeneity of GBM combined with its low incidence complicates the discovery of drugs that could benefit a large subset of patients [8, 9]. Thus, for example, while EGFR and PDGFR activation via amplification, and deletion mutations of NF1 and CDKN2A are each fairly common in GBM, different patients, and even different portions of tumor within a patient can manifest various combinations of these alterations, leading to differences in treatment response within and across tumors [13].

Thus the development of strategies that can thwart resistance amidst complex and heterogeneous signaling mechanisms is of prime importance. We approached this through a series of experiments aimed broadly at systematically quantifying the responses of GBM tumorsphere lines to targeted treatment combinations. Tumorsphere lines are derived from primary tumors using the neurosphere method, detailed later on in this thesis. They represent a relatively homogeneous and treatment resistant fraction of the original tumor that retains the genetic mutations of the parent tumor. Our goals in this study were

1) To identify synergistic pairs of drugs in three tumorsphere lines bearing genomic alterations representative of the signaling subclasses [4] of GBM tumors

    a. By determining the single drug dose response behavior of each drug in all three tumorsphere lines

    b. Evaluating the effect of combinations of equivalently inhibitory concentrations of each drug pair on the tumorsphere lines to calcu-

late two measures of synergy for each combination, defined later in this thesis

c. Nominating drug combinations for further study when they are both efficacious and synergistic

d. Relating the observations of combinatorial behavior made to known instances of drug interaction and prior biological knowledge in the realm of GBM and other related solid tumors

Predominant among the synergistic drug combinations we reported are the combination of MEK and AKT1/2 inhibition in TS543, a tumorsphere line that harbors a PDGFRA amplification, that of gefitinib (EGFRi) and AG538 (IGFRi) in TS565, which is NF1 deleted and of gefitinib and stattic (STAT3i) in TS676, a line bearing amplified EGFR as well as the EGFRvIII mutation.

Our second project sought to extend these results to a clinically defined subset of patients with GBM. We selected EGFR activated GBM as the subtype of choice for several reasons. Nearly 50% of GBM tumors harbor EGFR amplifications, and many of these tumors also have the EGFRvIII mutation, which is a deletion variant of the extracellular domain of EGFR that is constitutively active. However, the majority of patients do not benefit from receiving EGFR inhibitors in treatment. Further, the uses of high concentrations of EGFR targeted drugs in pre-clinical and in-vivo studies has revealed that the EGFR signaling network in this subset of GBMs may be sensitive to inhibition in the presence of sufficiently high concentrations of the drug [7]. In practice, such high concentrations of drug can be challenging to reach because of factors such as the BBB. One way to address this is by

combining EGFR inhibitors with other drugs that synergistically enhance cellular sensitivity to EGFR inhibition.

Another strategy for maximizing the observed synergy between two drugs is sequential administration [14-16]. Proteins change dynamically in time, both via post-translational modifications that can confer them with contextual functionality, such as by the phosphorylation of a receptor tyrosine kinase (RTK) on ligand binding, and via their signaling interactions with other functional proteins, often in different locations such as the mitochondria and nucleus. Thus the phenotypic consequences of inhibiting a protein are likely dependent on the predominant state/s of that protein at the time the inhibition is applied. In our second project, we treat the effect of dynamic protein variations on combination effects as an explicit variable, investigating the effectiveness of combinations delivered both simultaneously and sequentially. Specifically, our goals here were

2) To discover drugs that would cooperatively enhance the response of selected EGFR driven tumorsphere lines to treatment with lapatinib, a dual inhibitor of EGFR and HER2. This involved

    a. Identifying optimal "second hits" – targets whose inhibition might synergize with the effects of an EGFR inhibitor. Towards this, we explored the response of TS676 (EGFR++*) to a series of 7 single drug perturbations over time, using the data obtained to identify significant responders to treatment and time periods during which these responses were observed.

    b. Comparing the effects of simultaneous delivery of each combination with sequential administration in both orders and with different time delays, the selection of which was informed by our single

drug response data. This was performed using a resazurin cell viability assay.

c. Validating the observed sequence dependent synergy of lapatinib with the BCL2 inhibitor obatoclax using two additional phenotypic assays selected for their ability to measure features of drug effect that could not be measured using the Resazurin assay.

d. Extending the survey of this combination to other EGFR altered cell lines towards determining the dependence of these observations on (a) EGFR copy number and (b) the EGFRvIII mutation.

e. Quantifying the protein correlates of the observed synergies by analyzing the levels of 46 proteins in two EGFR altered GBM tumorsphere lines subjected to sequential and simultaneous inhibition by lapatinib and obatoclax.

This thesis is organized as follows. The remainder of this chapter introduces the background relevant to our work, going over the biology of GBM, therapeutic strategies and relevant clinical trials, and the methods we use to address our goals. The second and third chapters detail the rationale, protocols and results that constitute the two projects I described above. Finally, an appendix details a method for Reverse Phase Protein Array data normalization I developed[17].

Glioblastoma – the disease and molecular profiling

Glioblastoma (GBM) is the most frequent brain tumor and is almost always lethal. The median survival of patients with GBM is about 15 months [18], and disease progression is accompanied by cognitive decline, personality changes, and seizures, making the short survival period extremely challenging. Several groups

and consortia have dedicated their efforts towards cataloging the genetic variations represented across large groups of GBM tumors [1, 19]. We now know that GBMs cluster into a number of subtypes based on their mRNA expression patterns [20], and that these subtypes also show other aberrations that correspond with the known subtypes, such as the amplification of specific Receptor Tyrosine Kinases and mutations leading to the expression of such malfunctioning variants as EGFRvIII, PDGFRΔ8-9 and the NF1 deletion [21] [22]. In this section, we will go over the results of these studies and what we have learned from them about the pathophysiology of GBM. We will then discuss preclinical studies and clinical trials that have attempted to translate these findings to improvements in treatment.

In 2006, glioblastoma became the first tumor type to be studied exhaustively in a pilot study by The Cancer Genome Atlas, an initiative launched by the National Cancer Institute (NCI) and the National Human Genome Research Institute (NHGRI). The study integrated results from platforms present in 18 participating institutions, and included DNA sequencing, array CGH and mRNA expression data to identify mutations, copy number changes and transcript levels respectively [1]. The focus in this study was to identify novel and recurrent genetic alterations in untreated GBM tumors. The principal findings of this study were the identification of a small set of genes that showed recurrent mutations - TP53 (42%), PTEN (33%), NF1 (21%), EGFR (18%), RB1 (11%) and PI3K subunits (17%) [23]. Frequent amplifications of PDGFRA, EGFR and MET were also identified, and it was shown that they are largely mutually exclusive with one another.

Subsequent work on GBM by the TCGA led to the identification of transcriptionally defined subclasses - the Proneural, Classical, Neural and Mesenchymal sub-

types - based on the presence of signature genes within each class belonging to distinct developmental lineages of cells. While different transcriptomal signatures have been derived across different studies depending on the data and technique used, some strong and consistent observations emerged from these studies. For example, the Proneural subclass was associated with PDGFRA amplifications and TP53 and IDH1 mutations. 95% of the Classical samples showed EGFR amplifications and 95% showed a homozygous deletion of the Ink4a/Arf locus. Similarly, the Mesenchymal subtype showed high expression of CHI3L1 and MET, and a high frequency of NF1 mutations. The differences between the subtypes also had consequences for response to standard treatment regimens. Aggressive treatment most favorably affected survival in the Classical subtype but made no difference to the Proneural subtype [3].

Several questions arose naturally as a consequence. Could the differences between the subtypes be used to tailor therapies that targeted mutations specific to a subtype? Is there a single alteration or set of alterations that varies consistently across patients in a tumor-subclass dependent manner – a biomarker or signature that can be measured in patient material to assist the diagnosis and subsequent treatment of a patient's disease specific to subclass?

Molecularly targeted treatment of GBM

Partly because GBM was the first comprehensive project initiated by the TCGA, it is among the most thoroughly profiled cancers today. Careful studies of the results of the subtyping studies suggest that specific subclasses of patients (the IDH1 mutant and H3F3A mutant K27 subclass) have better survival and benefit less from aggressive chemotherapy [3, 22]. These patients comprise a very small

fraction of patients with GBM. Despite extensive study, therapeutic advances in GBM have lagged behind those in other cancers such as breast, lung and colon cancer [24]. What has hindered the translation of the findings from molecular studies into effective therapies?

Two broad classes of mechanisms contribute to resistance to therapy. The first is signaling network robustness, wherein proteins and genes that interact with the mechanism being inhibited are able to adaptively counterbalance the effect of inhibition. Similar mechanisms of signaling robustness have been known to operate across different types of cancer. One type of robustness is when a target is innately resistant to treatment because of modifications such as steric hindrance to inhibitor binding [25], alteration of ATP affinity [26] or altered active site structure [27, 28]. In the context of GBM, such mechanisms could be involved in the processes that maintain the activity of downstream markers of pathway activity even when a targeted protein such as EGFR is successfully inhibited [10].

Alternatively, extrinsic resistance results from the recruitment of signaling proteins removed from the target, such as by alternative RTKs that may be transcriptionally activated upon targeting a mutated RTK [29] or by the relief of feedback inhibition imposed by a protein downstream of the targeted drug [30]. An example of extrinsic resistance is encountered in BRAF-V600E melanoma, where tumors that are initially exquisitely sensitive to MEK inhibition [31] eventually acquire resistance by the by-pass mediated activation of ERK, requiring ERK inhibitors to maintain tumor suppression [32]. A similar mechanism of resistance is observed in colorectal cancer bearing BRAF V600E, with the difference being that these tumors are intrinsically resistant to the inhibition of the BRAF mutant via

8

rapid feedback mediated activation of EGFR. Tumors can also undergo clonal evolution over the course of treatment to develop treatment resistant subclones with newly acquired driver mutations [33].

The second class is comprised of pharmacological factors, such as the affinity of drug-target binding being altered by mutations or the inability of sufficient drug to reach the tumor site because of the blood brain barrier [7, 34]. Table 1 briefly summarizes the results of some clinical trials of targeted agents for GBM.

Combination therapy as a strategy for overcoming drug resistance

One strategy for overcoming resistance to various inhibitors is the use of combinations of inhibitors that together, may lead to long-term remission. Studies of multiple drug effects in vivo, accompanied by efforts to understand the mechanisms of these drugs began in the early 1950s. An early advocate of combinatorial regimens, Howard Skipper wrote in 1954 [37]:

It is apparent that rather detailed knowledge of a series of biochemical events (as well as alternative pathways) must be at hand before rational attempts at sequential blocking or concurrent blocking can be undertaken. Once adequate biochemical knowledge is at hand the second requirement is the existence of proper antagonists.

Table 1. Targeted therapy agents alone (adapted from Olson et al, 2014 [35])

DRUG	**TARGET**	**AUTHOR (YEAR)**	**Outcome**
Bevacizumab	VEGFR	Burkhardt (2012)	Median PFS 10mo
Cilengitide	α-Integrin	Gilbert (2012)	Median PFS 8 weeks (terminated; slow accrual)
Vorinostat	HDAC	Friday (2012)	Median OS 3.2mo
TLN-4601	RAS-MAPK	Mason (2012)	Median OS 5mo
Trabedersen	TGFβ2	Bogdahn (2011)	Median OS 10.9mo
Rilotomumab	HGF/SF	Wen (2011)	Median PFS 4.1wk
Romidepsin	HDAC	Iwamoto (2011)	Median PFS 8wk
Aflibercept	VEGFR	de Groot (2011)	Median PFS 12wk
COL-3	MMP	Rudek (2011)	No response
Perillyl Alcohol	RAS	da Fonseca (2011) [36]	Median OS 5.9mo
Erlotinib	EGFR	Raizer (2010)	Median PFS 2mo
Pazopanib	Multiple RTKs	Iwamoto (2010)	Median PFS 12wk
Cintredekin Besudotox	IL13	Kunwar (2010)	Median survival 36.4wk
Bevacizumab	VEGFR	Chamberlain (2010)	Median survival 8.5mo
Vorinostat	HDAC	Galanis (2009)	Median OS 5.7mo

Among the first studies of its kind to address the complexity of biological networks and its consequences for therapy, this study took place decades before the human genome was sequenced. Sequential blocking referred to the inhibition of a

series of enzymatic reactions that took place in serial order, in relative temporal proximity of each other, towards the activation or generation of a single product. On the other hand, concurrent blocking meant inhibiting two enzymes that activated or generated a product by two different pathways.
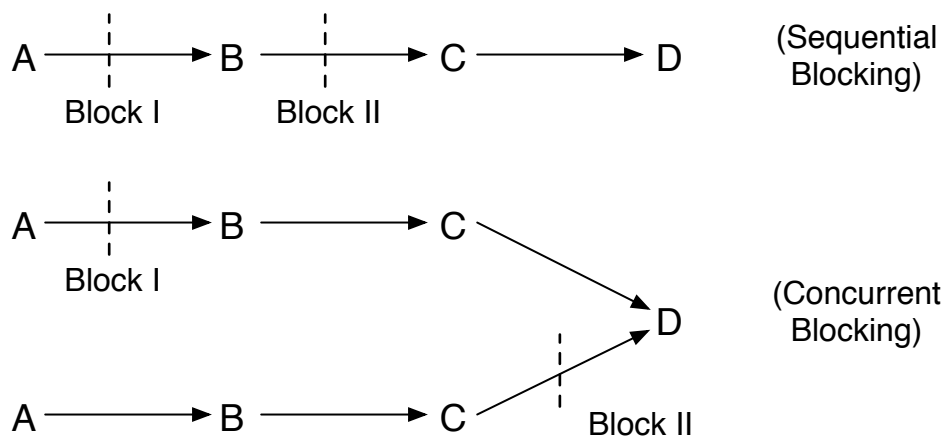
CHART 1. - DUAL BLOCKS PROVIDING SYNERGISTIC ACTIVITY
Reproduced exactly from H Skipper et al, Cancer Research 14(7), 1954

Figure 1. H. Skipper's representation of sequential and concurrent pathway blocking by drugs

In the years since this study, combination treatments have become extremely common in cancer therapy [38-41]. We have also learned much about the genetic drivers of cancer, and understanding the functional consequences of various mutations has allowed us to design therapies that target very specific alterations in cancer [42-44]. Yet, the benefit of combination chemo- and targeted therapies has largely remained restricted to a few cancers, and the acquisition of resistance is routine, even when drug combinations are used.

One promising approach for the study of disease networks is perturbation, often used in conjunction with data-intensive protein, metabolite and genomics platforms.

Perturbation to explore network dynamics in complex systems

Perturbation is an extremely powerful method for establishing relationships between the variables in a system of interacting elements. A perturbation applied to a gene or protein node in a cellular network can be used to model the effects of that node on its downstream effectors [45]. Genetic perturbation techniques such as the knockout and knockdown of genes are frequently used in molecular biology to assess the effects of individual genes on a network. While these methods are slow and laborious, more recent techniques such as high-throughput siRNA screens and CRISPR-Cas9 have revolutionized experimental biology, enabling the rapid and quantitative modeling of genetic events [46].

Another type of perturbation that can yield different types of information about cellular systems is the use of small molecules. Small molecules may be used to dynamically stimulate or inhibit selected nodes in a protein network and differ from genetic methods of perturbation in the following ways:

1) The concentration and method of delivery (impulse versus sustained) may be modulated to yield different degrees of inhibition or stimulation of a node.
2) Small molecules and antibodies may be engineered to bind to and affect specific sites in a protein, enabling the selective study of different aspects of that protein's function.

The phenotypic effect of perturbants on a network may also be of clinical interest. In fact, many perturbation studies are conducted to help model and understand disease physiology [47-50]. While single drug perturbation can be a very useful means of studying individual nodes in a network and the degree to which they affect cellular phenotype, most networks have evolved redundancy and robustness through feedback and cross-talk that limit their responsiveness to single perturbations. The use of multiple perturbations in this context may allow the inference of complex interactions between the nodes in a biological network [51, 52]. Using combinations of inhibitors also increases the amount of data that biologists are able to train inference algorithms with, increasing the descriptive and predictive power of the resulting models.

Tumorspheres as a model for GBM

One of the challenges of preclinical studies in GBM has been the identification of good models of the disease. GBM is characterized by heterogeneity and aspects of oncogenicity are maintained by interactions between cells bearing different mutations or levels of expression of certain proteins [13]. Inasmuch as the ability of a model to answer questions is limited by how closely it approximates the system under study, highly immortalized cell lines that have been established from human and mouse gliomas such as U-87 and U-251 differ from human GBM in the following ways:

1) Genetic drift with passaging leads to their losing many of the alterations observed in patient tumors [53]

2) Immortalization can lead to the acquisition of genetic changes not present in tumor [54, 55]

13

One hypothesis explaining the presence and maintenance of heterogeneity in GBM is the Cancer Stem Cell (CSC) hypothesis, according to which only a small subpopulation of cells in a tumor retains the ability to self-renew, differentiate and regenerate a tumor when transported to a favorable new environment. CSCs grow more slowly than the tumor bulk and often reside in the perivascular niche near the tumor periphery [56]. As a result, they are more resistant than the tumor bulk to chemotherapeutic agents that target mitotically active cells and to removal via surgery.

CSCs can be isolated using a protocol known as the neurosphere method [57, 58], which involves the repeated passaging of tumor derived cells in medium containing EGF and FGF but no serum, which selects for the undifferentiated component of the original population. CSCs in culture grow as spheroids also known as tumorspheres and are known to retain the alterations present in their parent tumors better than adherent differentiated cell lines [59, 60]. Once transplanted in vivo, they give rise to heterogeneity reminiscent of the parent tumor, enabling their use in both in vitro and in vivo contexts. This makes them good models with which to study drug resistance.

One disadvantage of using spheroid cell lines, like tumorsphere lines, is that cells may access different amounts of perturbants and nutrients depending on their depth within a neurosphere. This can introduce noise into the results that can make the interpretation of the results of subtle perturbations especially challenging. Pollard et al. devised a way to overcome this by growing GBM-derived tumorsphere lines on an ECM-associated substrate such as laminin [61]. When the-

se cells are grown in serum free medium, over a coating of laminin, they retain their stem-like characteristics and grow as adherent monolayers, making many experimental procedures less noisy and more convenient.

Phenotypic assays

Resazurin assay

The resazurin assay is a phenotypic assay used to provide a quantitative measure of the degree of aerobic respiration in a population of cells. This quantity may be used as a proxy for cell viability. It has been used to quantify bacterial content in foods and ecosystems [62, 63], and is routinely used in biomedical research to quantify the effects of various environmental stimuli and treatments [64]. Resazurin is a blue, weakly fluorescent compound, which when oxidized by active mitochondrial enzymes, fluoresces as the strongly red resosurfin.

We used resazurin to assess the effect of various drugs and drug combinations on cellular viability. In the most frequently used format, cells seeded in 96-well plates were subjected to various targeted drugs. Cellular activity was assessed after 3 days of treatment. Cell viability in response to drug treatment was quantified as cellular activity in the sample compared to the activity of the untreated control samples. For dose response measurements, a least-squares fit of the dose response data to sigmoidal response curves was performed using GraphPad PRISM version 6 for Mac and EC-50 values were obtained by interpolating the drug concentration corresponding to 50% viability compared to control. In other comparisons such as that of various combination treatments against each other, each condition was compared with the same untreated control. In all cases, the readings were background subtracted against a blank containing only growth

medium and resazurin reagent.

Reverse Phase Protein Arrays

Reverse phase protein arrays (RPPA) are a sensitive, sample-sparing immunological assay for the relative quantification of protein levels in a large number of samples. We used two types of RPPA technology for the experiments in this thesis.

The first method, referred to generically as protein lysate arrays, allows the simultaneous measurement of proteins in ~1000 samples across nearly 200 antibodies. The method was made available to us through a collaboration with the lab of Dr. Gordon Mills at the M.D. Anderson Cancer center. Proteins from lysed cells are spotted onto the surface of a nitrocellulose coated glass slide, which is then treated with primary antibody and a biotinylated secondary antibody. The primary antibody binds to sample spots in proportion with the amount of the protein of interest per spot. Each slide is washed gently with a biotinylated secondary antibody containing a recognition site for a Streptavadin-HRP (horseradish peroxidase) conjugate enzyme. This catalyzes a colorimetric reaction and generates a colored signal that can be converted to an intensity by imaging.

The detection system used ensures high sensitivity, and hence the protein from as few as 3 cell equivalents per spot can be detected by antibody. However, the dynamic range of the assay is inherently lower than that of methods like ELISA. To work around this limitation, each sample to be analyzed is spotted as a series of 5 dilutions. Further, RPPA technologies that utilize a colorimetric signal can have greater background than fluorescent RPPA. The quality of the data obtained are also limited by the quality of the image detection system used (in many cases

16

a tabletop scanner) and the uniformity with which the liquid handling systems in use expose different parts of each slide to the reagents utilized. Many methods exist for normalizing and improving the quality of data obtained via RPPA. We developed one such method to reduce the spatial variability introduced across the samples printed on a single slide and reported this method recently. Details of the method along with instructions for use are provided as an appendix at the end of this thesis.

The second method, which is lower in throughput but has higher sensitivity and accuracy is called the Zeptosens (Bayer AG) protein array platform. In this method, 100-400pg of protein lysate is spotted onto the surface of glass chips in four dilutions. The method uses planar waveguide technology [65] to reduce the scattering of light leading to reduced background signal and greater sensitivity. We performed these experiments in-house, using a robotic arrayer and chip reader provided by the manufacturers.

RPPA has been successfully used in clinical diagnostics and biomarker identification [66-69], and in projects similar to ours, for the identification of accurate molecular drug targets, as well as the examination of protein network theoretical models [70-72].

ViCell assay

The ViCell Cell Viability analyzer uses microscopy to detect the number of cells in a sample, and in conjunction with the trypan blue dye, allows for the accurate detection of the number of living and dead cells in a sample provided to the ma-

17

chine. Samples with the cells of interest are diluted in medium containing trypan blue, a dye that penetrates dead cells but is unable to enter living cells. The machine is able to analyze 10 samples at a time, and can count as few as 2E4 cells at a time, in 0.5ml of medium. This makes it best suited to measuring cells grown in large flasks or petridishes, or to multiwell plates of up to 24 wells.

Incucyte Cell Growth

The Incucyte ZOOM™ live cell imager (Essen Biosciences, USA) is a robotic microscope that can be housed within an incubator, enabling the continuous imaging of live cells grown in various formats including 96-well plates. The microscope is capable of capturing bright field as well as fluorescent images. In our application, we use bright field measurement to quantify the percentage of each image captured that is occupied by cells. Measuring the change in this quantity over time gives us a measure of the growth rate of the cells. Several groups have used this technology to quantify the responses of glioma and other cancer cell lines to perturbations [61, 73].

CHAPTER 2
CHARACTERIZING PHENOTYPIC RESPONSES TO TARGETED THERAPY IN GENETICALLY DISTINCT GBM TUMORSPHERE LINES

Introduction

The majority of targeted drugs used in clinical trials in GBM have shown little to no benefit on patient survival. One of the main reasons for this is the considerable inter- and intra-tumoral heterogeneity characteristic of the disease. Stratified clinical trials in subsets of patients genetically determined to be more likely to respond to a particular treatment are desirable but hard to conduct in practice because of the low total incidence of GBM and hence of each observed subset [74]. Additionally, retrospective analyses that attempt to correlate patients' catalogued alterations with their treatment response have not lead to consistent observations, indicating that there may be variability between patients carrying certain known driver mutations [75, 76]. In this context, the use of targeted combinations of drugs against representative GBM cell lines could be a useful strategy with which to identify effective treatments. The use of cell lines enables a large number of drug treatments to be tested simultaneously, in replicate, potentially increasing the efficiency and statistical significance of the results.

We investigated the effects of twelve targeted drugs and their combinations on three GBM tumorsphere lines displaying the hallmark alterations observed in each of the EGFR, PDGFR and NF1 signaling subtypes as defined by Brennan, C. and others [4]. Our goals were to identify drugs or drug combinations that would differentially inhibit specific cell lines, and to nominate successful drug combina-

tions for further study via computational analyses, to expedite the path to animal models and trials that might lead to their translation to clinical use.

Experimental design and methods

Resazurin assay

We used the resazurin assay, described in chapter 1, to evaluate the response of each cell line to the 12 selected drugs and their combinations in a 96-well plate format. Cell seeding densities and the duration of the experiment were optimized so that the signal obtained would lie in the linear range of the assay (fig 2, below)

Linear correlation between cell number and OD_{590} using resazurin dye
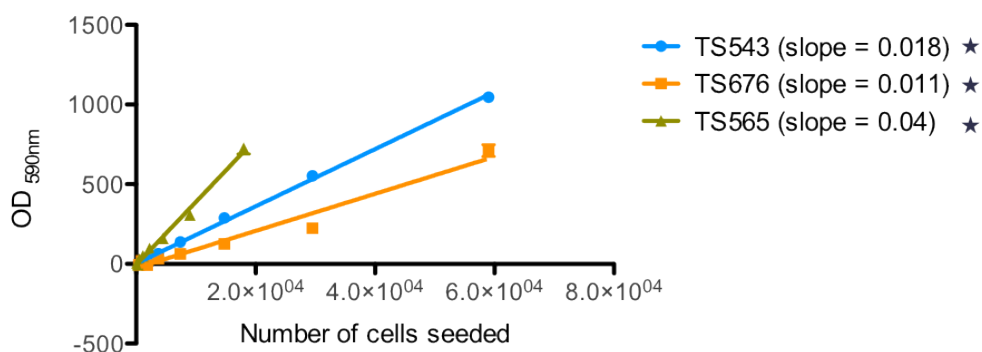
Figure 2. Linearity of resazurin assay within the range of cell numbers used in our drug treatment experiments

Tumorsphere model system

For our experiments, we used three tumorsphere lines derived from primary GBMs obtained in surgery by Dr. Brennan. The tumor material obtained was subjected to the progenitor cell selection using the methods previously described.
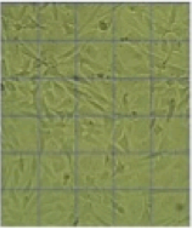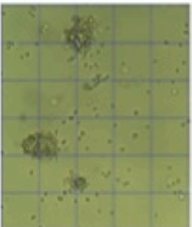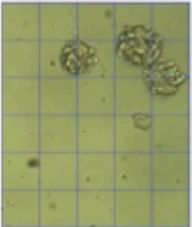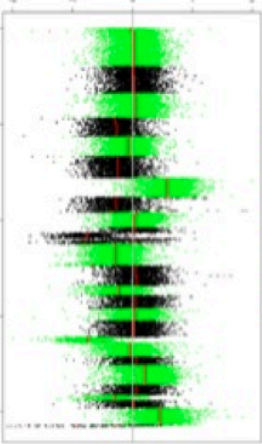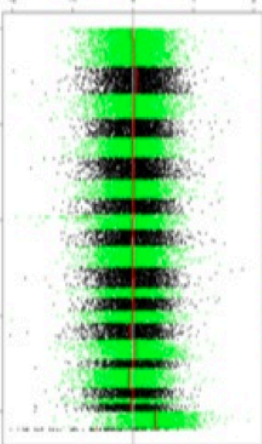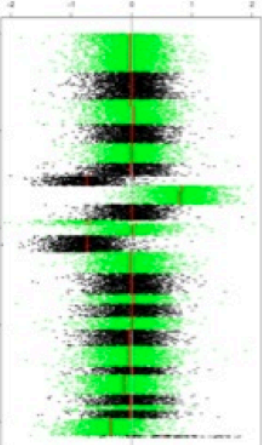
Array comparative genomic hybridization of the lines in early passages was used to determine the status of their driver copy number alterations such as EGFR, PDGFR, MET and MDM2/4. The copy number profiles of the tumorsphere lines used in this project are listed in table 3, along with representative images of the lines in their early passages.

Early passages of the lines were expanded into four passages without discarding any cells. The population that resulted was aliquoted into ~40 stock vials each that were cryogenically preserved for use in the remainder of this work. Analysis of the cells grown from these vials using SNP arrays in their 5th, 10th and 15th passages revealed that they continued to retain the driver alterations. In subsequent experiments, cells were only passaged 10 times after the thawing of a stock vial, after which the cells were discarded and a new vial used.

Single drug IC-50 evaluation

We first determined the concentrations of single drugs that could inhibit cell viability in the three cell lines. Our goal here was twofold. First, the nature of the dose response curve is instructive about the sensitivity of the cell line to the inhibition of that target. Further, we used the single drug dose response curves obtained to evaluate IC-50 (or IC-X% values where appropriate, for example when 50% inhibition was not reached) for comparison with the equivalent IC value for the combination. This enabled an evaluation of the synergy, additivity or antagonism of combinations. Methods for the evaluation of these are discussed in the

Table 2. Comparison of the three glioblastoma derived tumorsphere lines use din the study of drug combination responses.

Morphology	TS565	TS676	TS543
3-5 days after thawing Optical microscopy (100x)	Adherent	Grow in suspension Form small spheres that can adhere to the plate	Grow in suspension Form bigger spheres
Doubling time	~2 days	~1.9 days	~1.7 days
Genomic Alterations	--[CDKN2A,CDKN2C], with two NF1 mutations (c2195G>T, c470G>T) [38]	++[EGFR*,MDM4], +[MET,CDK6], --[PTPRD,PTEN], --CDKN2A*	++[PDGFRA,CDK4], +[EGFR,MET,CDK6], --PTEN
aCGH profile 15-20 passages after thawing (using 44k Agilent arrays)			
Subtype assigment	Mesenchymal NF1 subtype	Classical EGFR subtype	Proneural PDGFR subtype

next section. Cells seeded in 96-well plates were subjected to different concentrations of various targeted drugs. Cellular activity was assessed after 3 days of treatment. Cell viability in response to drug treatment was quantified as cellular activity in the sample compared to the activity of the untreated control samples. A least-squares fit of the dose response data to sigmoidal response curves was performed using PRISM software. IC-50 values were obtained by interpolating the drug concentration corresponding to 50% viability (w.r.t control). The results obtained are summarized in table 2.

Table 3. Comparison of the effects of various targeted single drugs on cell viability and protein activity in three glioblastoma tumorsphere lines.

Drug	Target	Observed cell-viability IC-50 (µM)			Antibody used	Lowest concentration at which protein inhibition is observed* (µM)		
		TS543	TS565	TS676		TS543	TS565	TS676
Gefitinib	EGFR	17.28, 13.1	3.2	No substantial inhibition	pP70S6K, pERK	pP70S6K & pERK rise with GF up to 10µM	No effect	0.37
AG53	IGF1R	No significant effect on cellular activity observed			pAKT	No effect	0.2	0.2
PDGF	PDGFR	4.1	3	No effect	pP70S6K	0.33	0.18	0.25
PD90	MEK1/2	No effect	35% inhibition at 100nM	No effect	pERK	No effect	25x10⁻³	No effect
SU11	MET	6.18, 5.16	6.3	6.13	pP70S6K	3	3	TBD
RO45	PKC	3.4	5.5	2.9	pP70S6K	No effect	1.25	2.4
SRCi	SRC	No effect	14.6	4.5	pAKT	44x10⁻³	20x10⁻³	15x10⁻³
AKT-VIII	AKT1/2	7.6	20% inhibition at 15µM	8.5	pAKT	0.2	No change in pAKT	0.4
ZSTK4	PI3K	0.46, 0.31	No effect	0.393	pAKT	14x10⁻³	No change in pAKT	60x10⁻³
Stattic	STAT3	4.22	No effect	2.66	pSTAT3	No effect	No effect	No effect
Ryuvidine	CDK4/6	1.5	1.26	0.8	pRB	1.5x10⁻³	3x10⁻³	1.5
Temsirolimus	mTORC1	0.07, 0.055	0.022	30% inhibition at 7.5nM	pP70S6K	0.55x10⁻³	0.4x10⁻³	0.5x10⁻³

Combination effect determination

To evaluate the effects of drug combinations on the cell lines, we subjected them to combinations of equivalently inhibitory concentrations of each drug obtained using the single drug dose response in each cell line. In some cases the single drugs did not reach equivalently inhibitory concentrations over the range of concentrations applied – this usually happened when one drug was very effective and was able to reduce cellular activity to near zero values compared with the untreated controls, whereas the other drug tested was relatively ineffective. In these cases, we still tested these combinations. However, our selection of the range of concentrations to apply in these cases were influenced by the literature, and we selected eight 1:2 or 1:3 serial dilutions centered around the literature derived IC-50 for these drugs.

Cells were seeded in 96 well plates and treated simultaneously with 8 combinations of the drugs in a 1:1 inhibitory concentration ratio. Cellular activity was assessed 3 days after treatment and the data obtained were fitted to sigmoidal dose response curves as in the single drug treatments.

Evaluation of drug combination effects

We observed that when drugs are combined, observed non-additive effects manifest either as changes in the effective dose required to cause a particular fractional change in cell viability, or as changes in the effective killing at particular doses applied. To identify cases of synergy and antagonism arising from both of these, we use two measures – the Combination Index (CI) [77] and the Efficacy Index – to quantify each drug combination.

The combination index (CI), uses Loewe Additivity [78] as its null model.

$$CI = \frac{[A]_{F_{a,AB}=X\%}}{[A]_{F_{a,A}=X\%}} + \frac{[B]_{F_{a,AB}=X\%}}{[B]_{F_{a,B}=X\%}}$$

Here $F_{a,C}$ indicates the fraction of cells **affected** by a condition c. Hence $[A]_{F_{a,AB}=X\%}$ indicates the concentration of A at which X% of the cells are affected under condition AB, i.e. when the drugs are combined. Each term in the sum is hence a ratio of the dose of a drug required to cause an effect X when in combination with another drug to the corresponding dose required when it is acting alone. The combination index of an additive combination evaluates to 1. Synergistic combinations have CI<1 and antagonistic combinations have CI>1. In the case where each individual drug has no effect, the denominators of the equation become extremely large and CI becomes 0, its lower limit. The CI of antagonistic combinations is positive but theoretically uncapped. The CI evaluated for a particular drug combination depends on the percentage X chosen at which to compare the effects of the single drugs with the combination. We follow convention and set X = 50%. When we do this, we observe that in some instances, it is not possible to evaluate CI, because even though the combination is effective at inhibiting cells, neither individual drug reduces cell viability by 50% or more. In such instances, we evaluate the effectiveness of a drug combination based on the change in cell viability that results from combining two drugs as compared to that caused by each drug alone.

We term this the efficacy index, EI, the ratio of the sum of the maximum observed fractions of cells affected by individual drugs to that observed when they are added to each other.

$$EI = \frac{F_{a,A} + F_{a,B}}{F_{a,AB}}$$

The efficacy index is only meaningful in those cases where the individual drugs reduce cellular activity by 50% or less. If the numerator exceeds 1, then an evaluation of the effect of the combination is impossible. In such cases, however, CI is sufficiently indicative of the degree of non-additivity. Within the allowed ranges for F_a however, EI behaves in the same way as CI for synergistic and antagonistic combinations, with EI=1 implying additivity, EI<1 implying synergy and EI>1 antagonism. The results of these evaluations are summarized in Figure 3.

Results

Combinatorial therapy reveals tumorsphere-line dependent synergies

We used the Loewe additivity criteria discussed earlier to evaluate combination indices, defined at 50% inhibition for all drug combinations. The combination indices obtained are demonstrated in the heatmaps below, colored in a blue-red scale mapping from synergy to antagonism. In cases where neither drug when used alone was able to inhibit cell viability by 50% or more, we evaluated the efficacy synergy instead. This enabled the identification of synergies such as that of gefitinib and SRCi in TS676, whose CI defined at 20% inhibition is evaluable but not high. However, as the combination has a much sharper effect on cell viability than do either of the component drugs alone, the efficacy synergy evaluates to < 1, revealing the synergy.

The strategy of using an efficacy index in addition to a combination index evalu
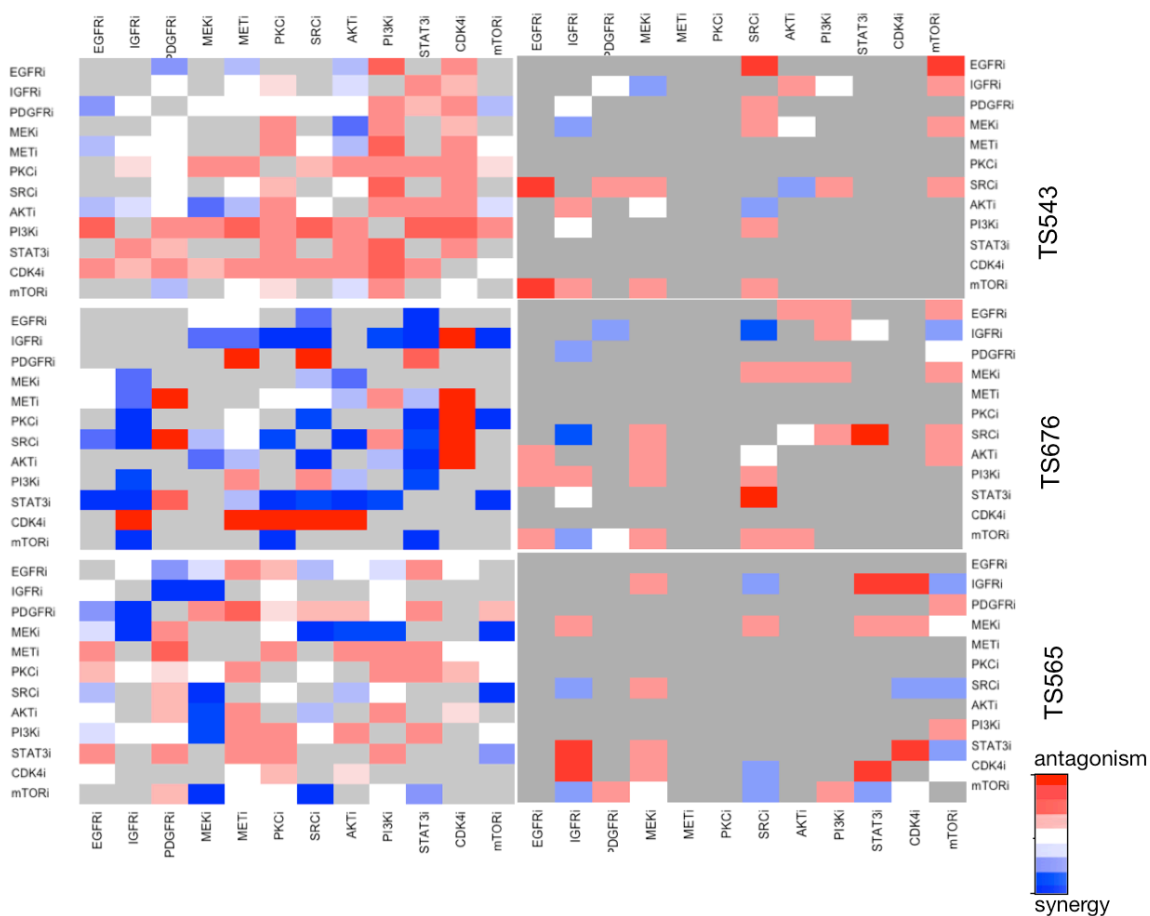
Figure 3. Heat map of combination and efficacy indices calculated in a 12 drug pair study

ated at 50% or greater inhibition is also relevant in the context of therapeutic use because some drug combinations can appear highly synergistic if their CI is eval-uated at lower effect levels despite low efficacy.

Other notable synergies observed were that of

(a) EGFRi (gefitinib) and STAT3i (stattic) in TS676. Subsequent studies have documented this synergy, not only in glioma [79] but also in ovarian and head and neck cancer [80, 81], indicating the broad therapeutic potential of the combination. In cases such as this combination, where one of the component drugs effectively reduced cellular activity by 50% or greater (in this case, STAT3), whereas the other reached a steady state above 50%, a combination index was evaluated by assigning an arbitrary extremely high value to the single drug IC-50 of this drug (in our case 1E64μM). This procedure also enabled the detection of these synergies that might otherwise have remained undetected.
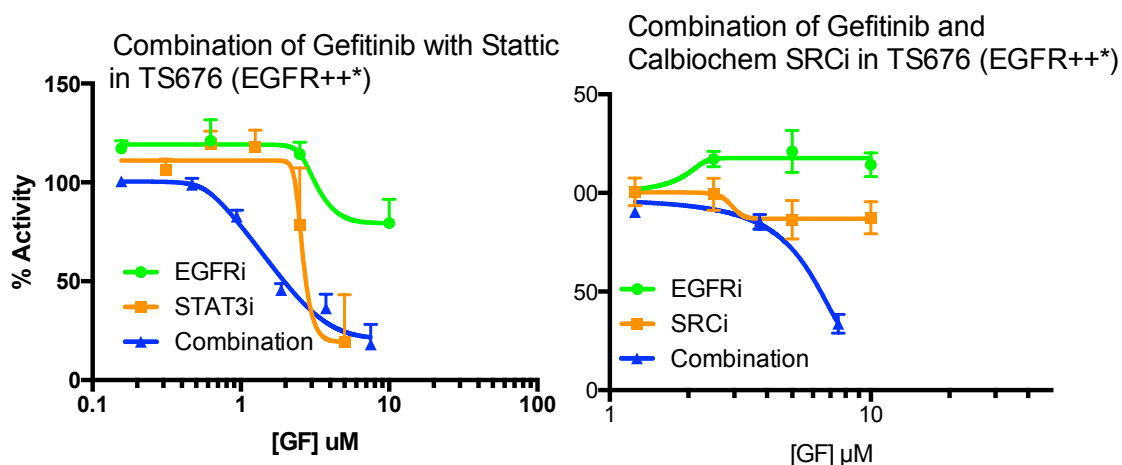
Figure 4. Dose response curve of the combinations of gefitinib with static (STAT3i) and gefitinib with PP1 (SRCi) in TS676

(b) MEKi (PD0325901) and PI3Ki (ZSTK474) in TS565, the NF1 deleted line. This synergy has also been observed in treatment resistant pancreatic cancer cell lines [82], colorectal cancer cell lines [83] and NRAS mutant melanoma cell lines and in vivo [84]. It has also been effective in vivo in models of castration resistant

prostate cancer [85], and malignant plural mesothelioma [86]. This drug combination was not synergistic in either of the other two lines.

The combination of ZSTK474 with PD0325901 was synergistic in the NF1 deleted TS565 but additive in EGFR amplified TS676 and PDGFR amplified TS543.
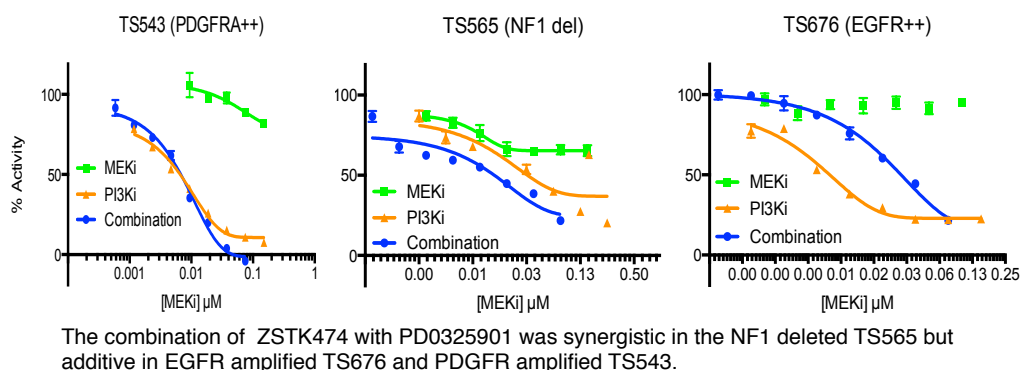
Figure 5. Differences between the effects of dual PI3K and MEK inhibition across the three tumorsphere lines

In fact, all three lines displayed relative insensitivity to gefitinib and the MEK inhibitor when used alone, with gefitinib displaying a biphasic dose response relationship and potentiating cell viability at low concentrations. This behavior of certain pharmacological agents, hormesis, is well documented in human cancer cell lines [87].

CHAPTER 3
SEQUENTIAL TREATMENT OF EGFR ACTIVATED
GLIOBLASTOMA CELL LINES

Introduction

Nearly 50% of GBMs have amplifications of the Epidermal Growth Factor Receptor (EGFR) that frequently co-occurs with mutations of EGFR [88, 89]. The most common of these mutations is EGFRvIII, a deletion mutant of exons 2-7 in the extracellular domain of the protein [88]. While the mutation renders the receptor incapable of binding to ligand, the variant displays low-grade constitutive activity. The mutation also reduces the rate at which the receptor is internalized [90], increasing its surface signaling to downstream receptors. Consequently, these GBM tumors display a pathophysiology that is characterized by overactive and aberrant EGFR signaling, inhibiting which could be a potent therapeutic strategy.

In reality, attempts to inhibit EGFR biochemically have shown little to no benefit on survival in clinical trials of GBM [7, 91]. Several groups have attempted to understand the reasons for this and identify biomarkers of response. The early discovery of PTEN activity as a marker of response to EGFR inhibition [6] was among the first to implicate bypass mechanisms in the acquisition of resistance, but reproducing these findings in subsequent work has been challenging [92, 93]. Since then, many other groups have investigated the mechanisms of resistance to EGFR inhibition in GBM [94-96] but the findings remain to be translated clinically.

One approach for tackling resistance or lack of response to EGFR inhibitors in GBM has been to learn from other cancers with similar drivers. EGFR is critically important to oncogenic signaling in tumors such as lung adenocarcinoma and colorectal cancer, and the use of EGFR-targeted small molecules and antibodies has been relatively successful in these cancers [97-99], improving survival by up to a year even though acquired resistance eventually emerges. On the other hand, EGFR inhibitors in GBM have shown little survival benefit in the clinical setting. What are the differences between these two types of EGFR driven cancers and how do they impact how we address treatment resistance in GBM?

The majority of EGFR mutations observed in lung cancer occur in the intracellular kinase domain of the receptor, relieving the receptors of the autoinhibition that normally limits activity subsequent to receptor dimerization and causing up to 50-fold increases in activity [100]. Reversible small molecule inhibitors such as Gefinitib and Erlotinib bind to the ATP binding domain of this receptor, thus inhibiting autophosphorylation and downstream signaling [101, 102].

On the other hand, EGFR mutations in GBM occur most frequently in the extracellular domain, in the form of the deletion variant EGFRvIII. This mutation often co-occurs with EGFR amplification, resulting in high levels of both EGFR WT and EGFRvIII, and the two have been hypothesized to potentiate each other, resulting in the activation of downstream signaling pathways. Thus, utilizing inhibitors that are able to successfully reduce activity of the EGFRvIII variant could improve response in this subset of patients [7].

Another obstacle to the adequate inhibition of EGFR in GBM is the presence of the blood brain barrier, which may prevent sufficiently high concentrations of inhibitor from reaching the brain. In a study by Hegi et al., patients who had been treated with the EGFR inhibitor gefitinib preoperatively had their tumors examined for the drug after its removal by surgery [10]. The concentration of drug observed (4.1μg/g) while higher than that in plasma, was well below the concentration required to adequately inhibit EGFR phosphorylation in vitro, in representative cell lines [13].

Finally, one class of resistance mechanisms arises from signaling pathway robustness. These occur as a consequence of network features such as redundancy, feedback control and cross-talk between proteins that evolved as a consequence of their granting resilience to organisms in the face of environmental insults, but that are co-opted by the evolutionary processes leading to cancer. One way to disrupt these sorts of interactions is the use of drug combinations that alter the protein activities contributing to a phenotype. In this context, it has been shown taking the time at which each target is inhibited into explicit consideration can be a useful strategy. Protein interactions are dynamic in nature and robustness is often the result of compensatory processes that evolve over time in response to perturbations [103]. Thus the sequential treatment of cancer with drug combinations has been more effective than co-treatment in several tumors [14, 15, 104]

A therapeutic strategy is more likely to be effective if tailored to the constellation of resistance mechanisms unique to EGFR activated GBM. One such approach is the use of a second drug in combination with an EGFR inhibitor known to bind effectively to both WT and vIII forms of EGFR. An appropriately selected drug

33

could act synergistically with the EGFR inhibitor, lowering the amount of either drug required to levels that are achievable within GBM tumors. Successful combinations in this context would also likely disrupt the protein interactions mediating signaling robustness, as discussed earlier.
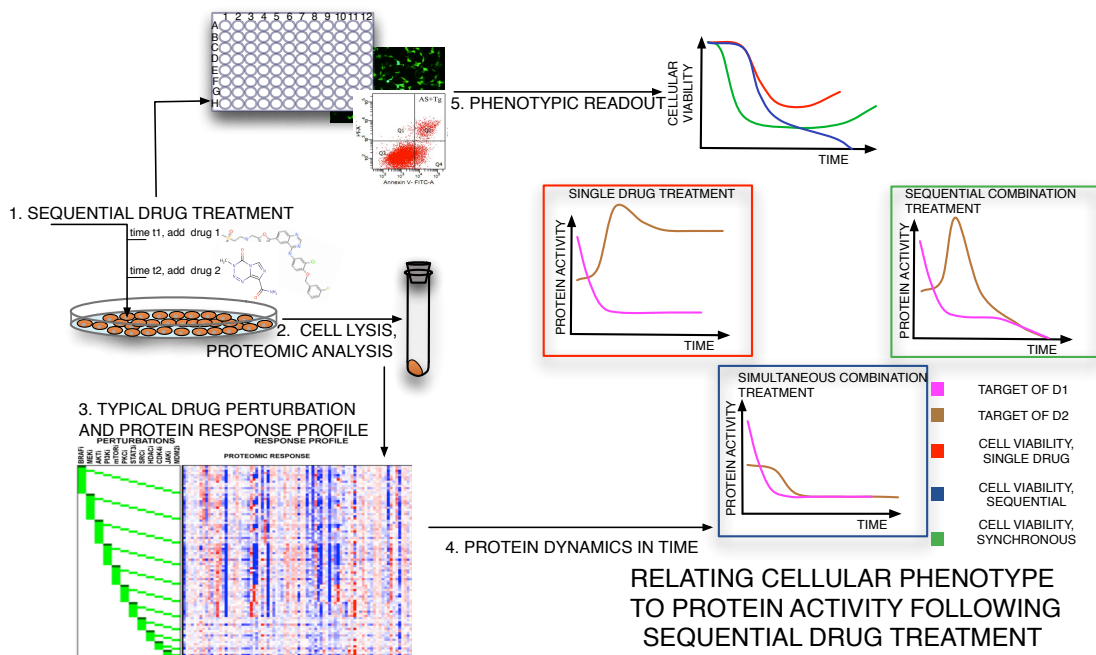
Figure 6. Graphical representation of the experimental design of sequential synergy experiments

Several groups have investigated the potential therapeutic benefits of combining EGFR inhibitors with other targeted and chemotherapeutic drugs. One such effort, in cell lines and a xenograft model from triple negative breast cancer, showed not only that the effects of EGFR inhibitors such as gefitinib, erlotinib and lapatinib could be improved bycombining them with the DNA alkylating doxorubicin, but that the order and time of drug application affected the observed synergy. Pretreatment with erlotinib enhanced the effects of the chemotherapeutic

drug in TNBC cell lines whereas the reverse order reduced the combination's effect. Similarly, in two large studies performed in breast cancer, glioblastoma and medulloblastoma cell lines, pretreating these lines with obatoclax enhanced the effects of the EGFR and HER2 inhibitor lapatinib in PTEN deficient cell lines. This work convincingly demonstrated the inhibition of processes downstream of the targets of each drug. However, the interaction of their effects towards the effects observed remains to be understood.

Using high throughput phenotypic screening of an EGFR amplified and EGFRvIII bearing tumorsphere line to combinations of drugs that include lapatinib, we showed that lapatinib was synergistic in combination with obatoclax and RO-31-7549 and that these drug combinations were effective at inhibiting cell viability. The observed efficacy of drug combinations is dependent not only on the sequence of drug administration but also on the time between drug perturbations. Further exploration of the combination of lapatinib and obatoclax in other EGFR altered cell lines (TS600 with a single EGFR gain and GBM39 with EGFRvIII and amplification) showed that while the drug combination remained effective and synergistic in all cell lines, its dependence on sequence and time delay was cell-line specific. We performed a protein array experiment that measured the responses of 60 proteins and phosphoproteins to lapatinib and obatoclax administered alone as well as in simultaneous and sequential combinations to explore the protein correlates of our phenotypic observations.

Experiments and results

I. Diversity of temporal dynamics after single drug perturbation of TS676

Rationale

Successfully perturbing a signaling network with sequentially administered drugs is critically dependent on the selection of appropriate times at which to perturb the selected targets [14]. We reasoned that observing the dynamics of protein response to single drugs that we were interested in using in combination with one another would assist the prospective selection of optimal time delays. We began our analyses with the GBM tumorsphere line TS676, an EGFR amplified cell line bearing the EGFRvIII variant in addition to an MDM4 amplification and a CDKN2A deletion. We perturbed this cell line with 7 single drugs and the ligand EGF at 10 time points spaced exponentially between 6 minutes and 2days. The selection of time points was based on observations from prior work showing that phosphoprotein responses to perturbants can manifest within minutes of treatment [105, 106], whereas total protein level changes, modified by longer acting phenomena such as transcription factor mediated gene regulation that occur over a period of hours to days. Further, the concentrations of the drugs applied corresponded closely to their IC-50 values, obtained from our evaluations in-house as well as from the literature, reported in table 2. In many cases, our selected concentrations were below those frequently chosen in experiments focused on detecting the phenotypic effects of these drugs. As our intent in this experiment was to identify proteins whose activities changed specifically in response to each drug applied, we used them in regimes that we anticipated would minimize promiscuous binding and other effects related to non-specificity.

Experiment protocol

Beginning at two passages before each experiment, cells were grown in flasks pre-coated with laminin (Sigma L2020) to enable the growth of tumorspheres as adherent monolayers. We used DME-F12 medium supplemented with B27, EGF and FGF (20ng/ml each) and heparin. Cells were seeded in laminin coated 6 well plates 12 hours prior to drug application. At the selected times after drug application, the plates were transferred to an ice-trough where the cells were rapidly scraped off each well, pelleted and frozen. Subsequently they were lysed and the protein fraction of the lysate was diluted appropriately for analysis using reverse phase protein arrays.

Data acquisition and normalization

Protein activities obtained using RPPA are reported relative to each other and to positive control spots printed uniformly on each slide. This allows the relative quantification of a protein's activity across treatments or conditions. We first apply a spatial normalization routine to the raw intensities obtained that removes spatial non-uniformity imposed on the measurements by factors such as uneven exposure of slides to experimental reagents [17]. Next, to map the quantified intensities to relative protein concentrations, we use a joint estimation method called SuperCurve [107] that fits all the sample intensities on each slide to a 3 parameter logistic equation.

Thus, each slide is associated with both global parameters and protein concentration estimates. The estimates obtained across all proteins are now normalized by median normalization and then rescaled by dividing them by the second median

obtained for each treatment across all protein values. The procedure is termed double median normalization.

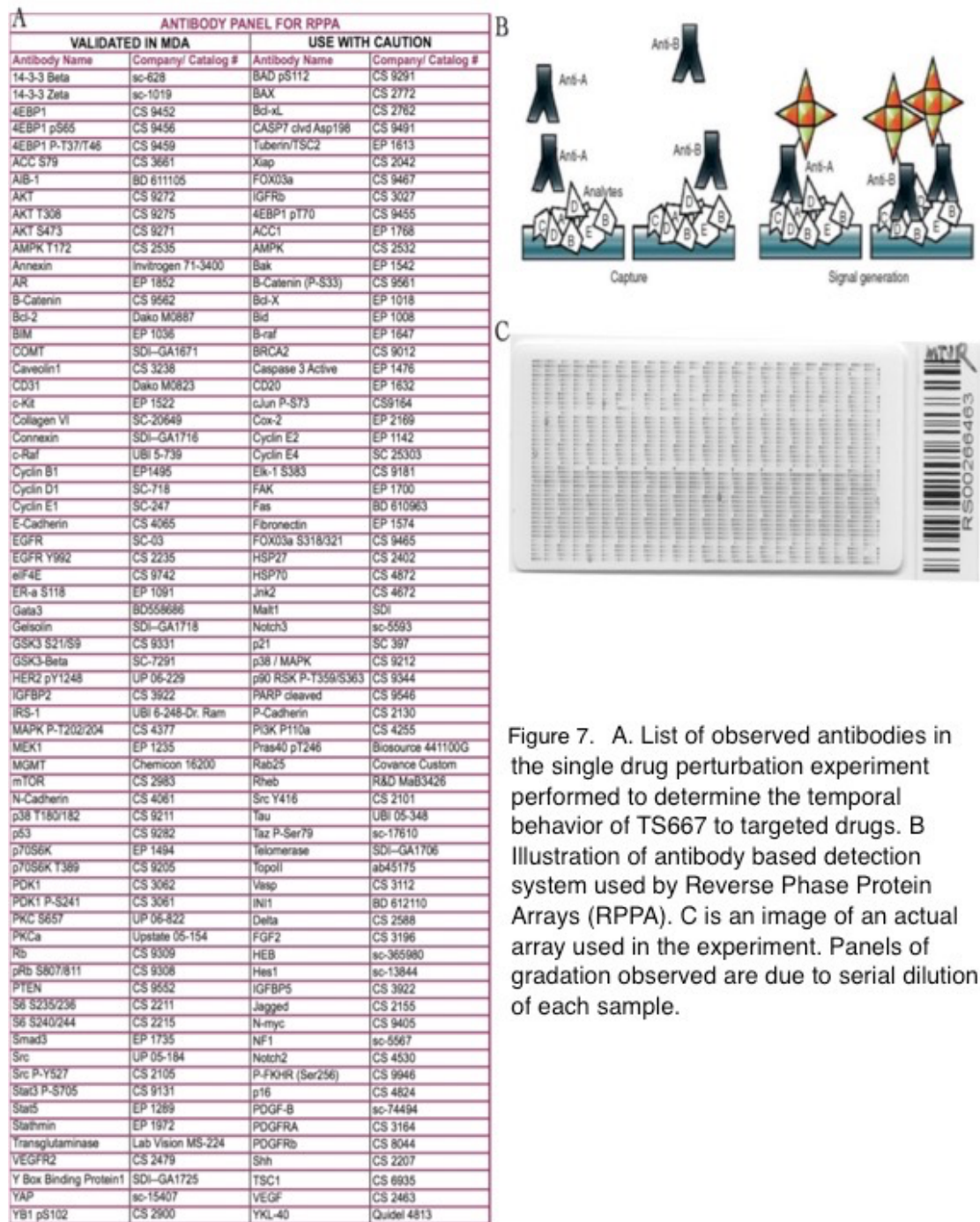| ANTIBODY PANEL FOR RPPA			
VALIDATED IN MDA		USE WITH CAUTION	
Antibody Name	Company/ Catalog #	Antibody Name	Company/ Catalog #
14-3-3 Beta	sc-626	BAD pS112	CS 9291
14-3-3 Zeta	sc-1019	BAX	CS 2772
4EBP1	CS 9452	Bcl-xL	CS 2762
4EBP1 pS65	CS 9456	CASP7 clvd Asp198	CS 9491
4EBP1 P-T37/T46	CS 9459	Tuberin/TSC2	EP 1613
ACC S79	CS 3661	Xiap	CS 2042
AIB-1	BD 611105	FOXO3a	CS 9467
AKT	CS 9272	IGFRb	CS 3027
AKT T308	CS 9275	4EBP1 pT70	CS 9455
AKT S473	CS 9271	ACC1	EP 1768
AMPK T172	CS 2535	AMPK	CS 2532
Annexin	Invitrogen 71-3400	Bak	EP 1542
AR	EP 1852	B-Catenin (P-S33)	CS 9561
B-Catenin	CS 9562	Bcl-X	EP 1018
Bcl-2	Dako M0887	Bid	EP 1008
BIM	EP 1036	B-raf	EP 1647
COMT	SDI-GA1671	BRCA2	CS 9012
Caveolin1	CS 3238	Caspase 3 Active	EP 1476
CD31	Dako M0823	CD20	EP 1632
c-Kit	EP 1522	cJun P-S73	CS9164
Collagen VI	SC-20649	Cox-2	EP 2169
Connexin	SDI-GA1716	Cyclin E2	EP 1142
c-Raf	UBI 5-739	Cyclin E4	SC 25303
Cyclin B1	EP1495	Elk-1 S383	CS 9181
Cyclin D1	SC-718	FAK	EP 1700
Cyclin E1	SC-247	Fas	BD 610963
E-Cadherin	CS 4065	Fibronectin	EP 1574
EGFR	SC-03	FOXO3a S318/321	CS 9465
EGFR Y992	CS 2235	HSP27	CS 2402
eIF4E	CS 9742	HSP70	CS 4872
ER-a S118	EP 1091	Jnk2	CS 4672
Gata3	BD558686	Malt1	SDI
Gelsolin	SDI-GA1718	Notch3	sc-5593
GSK3 S21/S9	CS 9331	p21	SC 397
GSK3-Beta	SC-7291	p38 / MAPK	CS 9212
HER2 pY1248	UP 06-229	p90 RSK P-T359/S363	CS 9344
IGFBP2	CS 3922	PARP cleaved	CS 9546
IRS-1	UBI 6-248-Dr. Ram	P-Cadherin	CS 2130
MAPK P-T202/204	CS 4377	PI3K P110a	CS 4255
MEK1	EP 1235	Pras40 pT246	Biosource 441100G
MGMT	Chemicon 16200	Rab25	Covance Custom
mTOR	CS 2983	Rheb	R&D MaB3426
N-Cadherin	CS 4061	Src Y416	CS 2101
p38 T180/182	CS 9211	Tau	UBI 05-348
p53	CS 9282	Taz P-Ser79	sc-17610
p70S6K	EP 1494	Telomerase	SDI-GA1706
p70S6K T389	CS 9205	TopoII	ab45175
PDK1	CS 3062	Vasp	CS 3112
PDK1 P-S241	CS 3061	INI1	BD 612110
PKC S657	UP 06-822	Delta	CS 2588
PKCa	Upstate 05-154	FGF2	CS 3196
Rb	CS 9309	HEB	sc-365980
pRb S807/811	CS 9308	Hes1	sc-13844
PTEN	CS 9552	IGFBP5	CS 3922
S6 S235/236	CS 2211	Jagged	CS 2155
S6 S240/244	CS 2215	N-myc	CS 9405
Smad3	EP 1735	NF1	sc-5567
Src	UP 05-184	Notch2	CS 4530
Src P-Y527	CS 2105	P-FKHR (Ser256)	CS 9946
Stat3 P-S705	CS 9131	p16	CS 4824
Stat5	EP 1289	PDGF-B	sc-74494
Stathmin	EP 1972	PDGFRA	CS 3164
Transglutaminase	Lab Vision MS-224	PDGFRb	CS 8044
VEGFR2	CS 2479	Shh	CS 2207
Y Box Binding Protein1	SDI-GA1725	TSC1	CS 6935
YAP	sc-15407	VEGF	CS 2463
YB1 pS102	CS 2900	YKL-40	Quidel 4813

Figure 7. A. List of observed antibodies in the single drug perturbation experiment performed to determine the temporal behavior of TS667 to targeted drugs. B Illustration of antibody based detection system used by Reverse Phase Protein Arrays (RPPA). C is an image of an actual array used in the experiment. Panels of gradation observed are due to serial dilution of each sample.

38

Results

We observed that proteins fell into three broad categories, displaying local maxima and minima early (6min-0.5h), intermediately (1.5h-6hours) or late (>12h) after treatment. To identify those proteins whose activities were the most affected by treatment, we computed the area under the time series curve (AUC) for each protein in response to every treatment and compared this to the corresponding AUC of that protein's time course in the absence of treatment. We identified proteins showing an absolute change in AUC of 25% or greater compared to untreated control as 'responders' if this response was statistically significant across all three replicates of the time course measured. For this, we used a two tailed t-test, assessing the level of significance of the p-values obtained by comparing them with the level of significance obtained from a 1% FDR-permissive Storey test. The list of responders across each protein is in Table 3.

Some of our specific observations were

(a) Lapatinib treatment is associated with the late induction of BIM in TS676

(b) Obatoclax and PKCi are associated with an intermediate induction of pAKT-pS473.

Both Western Blots and Zeptosens RPPA data validated the latter of these observations. However, in both cases, pAKT continued to increase after 6 hours up to 24hours. This discrepancy could be because of experimental error in the first RPPA experiment, where we had to deal with multiple samples and temperature or other effects could have introduced noise into the results. Further the MDA RPPA platform is inherently noisy because of factors discussed earlier. As the western blots were repeated and Zep-

tosens arrays are less error prone than MDA-RPPA, we are confident that pAKT levels rise over the period of a day in response to obatoclax.

Changes in the levels of proteins downstream of the targets of lapatinib and obatoclax observed between 6 minutes and 1 day after inhibition. lapatinib treatment leads to the inhibition of pAKT whereas obatoclax potentiates it. This observation was validated by subsequent experiments including Western Blots
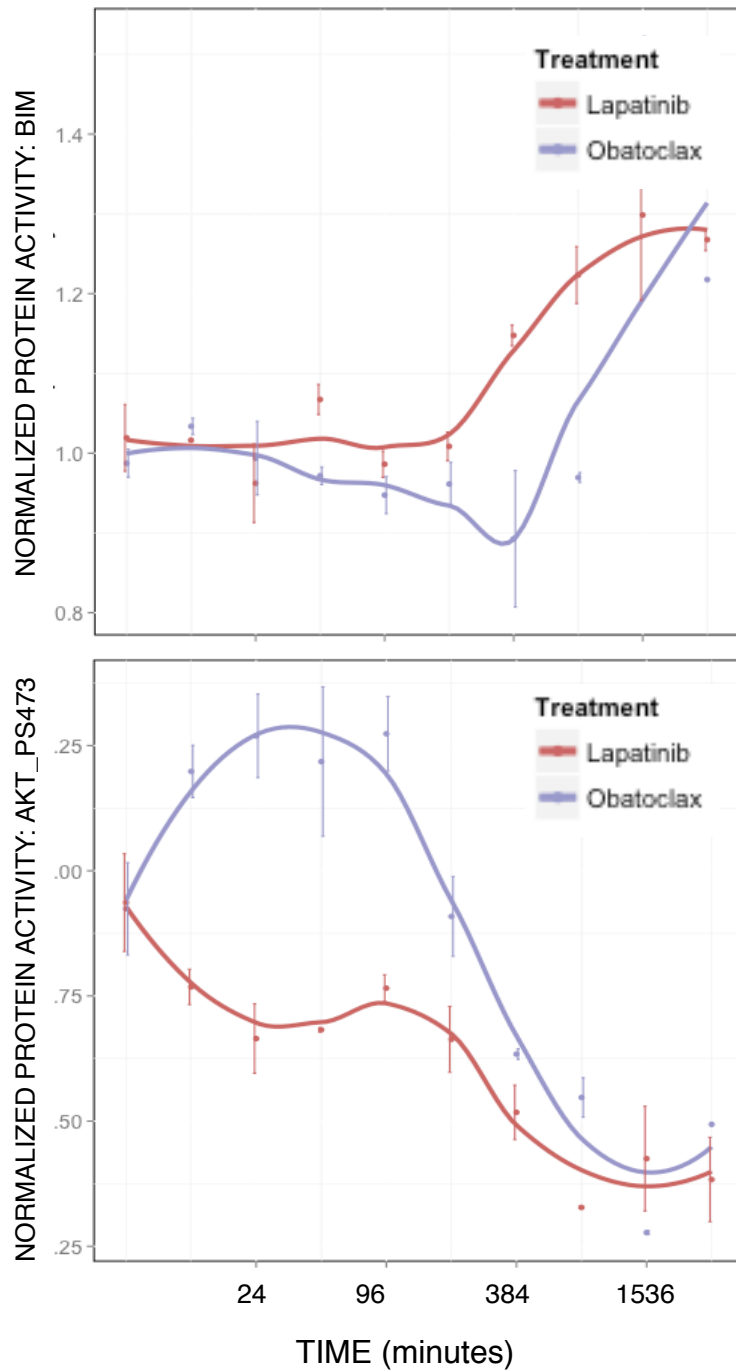
Figure 8. Responses of the proteins pAKT and BIM to single drug application with lapatinib and Obatoclax

Table 4. Statistically significant responders to single drug treatments identified by comparing the ratio of the area under each protein's time series curve to that of the protein's untreated control curve. A two-tailed t-test was used to determine significance across 3 replicates

TIME	ANTIBODY	TREATMENT	AUC ratio	p-value	MEAN DIFF
med	p38_pT180_Y182	Obatoclax	1.6277686	0.0011	-896.739
early	p38_pT180_Y182	Obatoclax	1.4410454	0.0008	-1284.38
early	MEK1_pS217_S2	Obatoclax	1.4064922	0.0016	-980.234
early	Rab11.R.E	Lapatinib	1.3574756	0.0016	-808.125
med	MEK1_pS217_S2	RO-31-7549	1.354577	0.0014	-733.933
early	C.Raf_pS338.R.E	Obatoclax	1.3144994	0.0014	-3109.14
late	Rab11.R.E	Obatoclax	1.3132368	0.0006	-243.664
med	c.Kit.R.V	Temozolomid	1.2987036	0.0008	-598.4
early	Rab11.R.E	PD0332991	1.2917168	0.0015	-808.766
med	JNK_pT183_pT18	Obatoclax	1.2883029	0.0019	-651.191
early	Rab11.R.E	Curcumin	1.2830512	0.0015	-808.85
med	c.Kit.R.V	Curcumin	1.2811378	0.0006	-601.052
med	MEK1_pS217_S2	Curcumin	1.2807678	0.0016	-748.594
med	MEK1_pS217_S2	BEZ-235	1.2778012	0.0014	-749.183
late	PKC.delta_pS664	Lapatinib	1.2777283	0.0002	-1415.04
early	PI3K.p110.alpha.	Lapatinib	1.2740156	0.0002	-1127.41
med	p38_pT180_Y182	RO-31-7549	1.2737422	0.0010	-986.039
med	Notch1.R.V	Obatoclax	1.2705029	0.0007	-1525.91
late	HER3_pY1298.R.(	BEZ-235	1.2699474	0.0012	-1239.84
med	p90RSK_pT359_S	BEZ-235	1.2647174	0.0008	-1356.96
early	c.Kit.R.V	Curcumin	1.2638852	0.0001	-782.209
early	Rab11.R.E	Obatoclax	1.254467	0.0015	-809.129
early	Rab11.R.E	BEZ-235	1.2544271	0.0016	-809.129
early	RBM15.R.V	RO-31-7549	0.7499868	0.0008	-25478.3
late	Akt.R.V	PD0332991	0.7444625	0.0015	-21568.3
med	RBM15.R.V	Curcumin	0.7365044	0.0009	-21950
early	Akt.R.V	EGF	0.7338995	0.0012	-32923.8
early	RBM15.R.V	Obatoclax	0.7305153	0.0008	-25485
early	eIF4G.R.C	PD0332991	0.7301565	0.0011	-24675.7
early	Akt.R.V	RO-31-7549	0.7296427	0.0012	-32925.9
overall	mTOR_pS2448.R	RO-31-7549	0.728994	0.0001	-762.2
late	Akt.R.V	Lapatinib	0.7276539	0.0001	-21833
early	Akt.R.V	BEZ-235	0.7263001	0.0012	-32927.6
overall	Akt.R.V	Lapatinib	0.7175975	0.0002	-9402.11
early	PRAS40_pT246.R	BEZ-235	0.7165496	0.0011	-6534.68
med	Akt.R.V	Lapatinib	0.7153165	0.0016	-27664.5
early	RBM15.R.V	Curcumin	0.7094862	0.0008	-25492.2
med	eIF4G.R.C	PD0332991	0.7077669	0.0016	-21118.7
early	Akt.R.V	PD0332991	0.7032897	0.0012	-32939.2
med	TSC1.R.C	PD0332991	0.6868866	0.0006	-25309.9
med	Akt.R.V	BEZ-235	0.6813607	0.0012	-27931.7
late	mTOR_pS2448.R	RO-31-7549	0.6749901	0.0002	-1833.85
late	eIF4G.R.C	Obatoclax	0.6740922	0.0013	-16368.8
med	PRAS40_pT246.R	BEZ-235	0.6648197	0.0013	-5682.67
early	Akt.R.V	Obatoclax	0.6647895	0.0012	-32958.6
late	Myosin.IIa.pS194	Lapatinib	0.6645339	0.0009	-23250
med	eIF4G.R.C	BEZ-235	0.6560012	0.0008	-21394.8
overall	IGFBP2.R.V	BEZ-235	0.6499928	0.0014	-4355.6
early	GSK3.alpha.beta_	RO-31-7549	0.647414	0.0016	-2170.22
early	Akt.R.V	Curcumin	0.646385	0.0012	-32967.8
med	Akt.R.V	Curcumin	0.6435094	0.0015	-28229.5
late	Akt.R.V	Obatoclax	0.6416966	0.0014	-23186.8
late	Tuberin.R.E	Obatoclax	0.6328233	0.0018	-13618
late	PRAS40_pT246.R	Obatoclax	0.6281506	0.0013	-4427.85
late	mTOR_pS2448.R	Obatoclax	0.6220387	0.0004	-1910.62
early	YAP_pS127.R.E	RO-31-7549	0.6178186	0.0014	-6124.71
late	mTOR_pS2448.R	BEZ-235	0.5877526	0.0005	-1960.33
overall	mTOR_pS2448.R	BEZ-235	0.5626977	0.0002	-1229.9
med	mTOR_pS2448.R	BEZ-235	0.5309018	0.0011	-2504.97
overall	eIF4G.R.C	BEZ-235	0.5189625	0.0007	-11975.1
late	eIF4G.R.C	BEZ-235	0.4522254	0.0011	-19174.8

II. Time delay dependent modulation of response to lapatinib by obatoclax

Rationale

We looked to our observations from the single drug time series responses to se-
lect both drug targets and delay times for a phenotypic screen aimed at evaluat-
ing the effects of a set of sequential drug combinations. Based on our observa-
tions that the greatest number of observed nodes changed by > 25% w.r.t un-
treated control during the intermediate time period (1.5-6h), we chose 6h as one
of the delay periods between drug applications to use in a screen. To incorporate
effects that might arise from targeting proteins that have equilibrated to steady
state levels imposed by the action of the first drug, we contrasted the selection of
6h with a second delay period of 24 hours.

Drug choice was motivated by network considerations such as the proximity of
the second target to perceived/prior knowledge of pathway structure. Thus we
selected drugs whose targets were proximal to EGFR, the target of lapatinib, such
as a PI3 kinase inhibitor or inhibited possible bypass activators, such as a PDGFR
inhibitor. We selected the cytotoxic drug doxorubicin, to enable a comparison of
our results with those of Lee et al [14], and Curcumin - a drug with several attrac-
tive targets including NFkB and COX-2. Finally, we included drugs with targets
distant from EGFR, such as the BCL2 inhibitor obatoclax and the STAT3 inhibitor
stattic.

Experiment protocol

Cells were seeded in 96 well plates at nearly 50% confluence. After 12 hours, they were treated with drugs, either as single perturbations, or in sequential or simultaneous combinations with lapatinib. After 3 days from the first treatment, cell viability across all measured conditions was evaluated using a resazurin assay. Cellular activity under each condition as reported as a fraction of the untreated control.
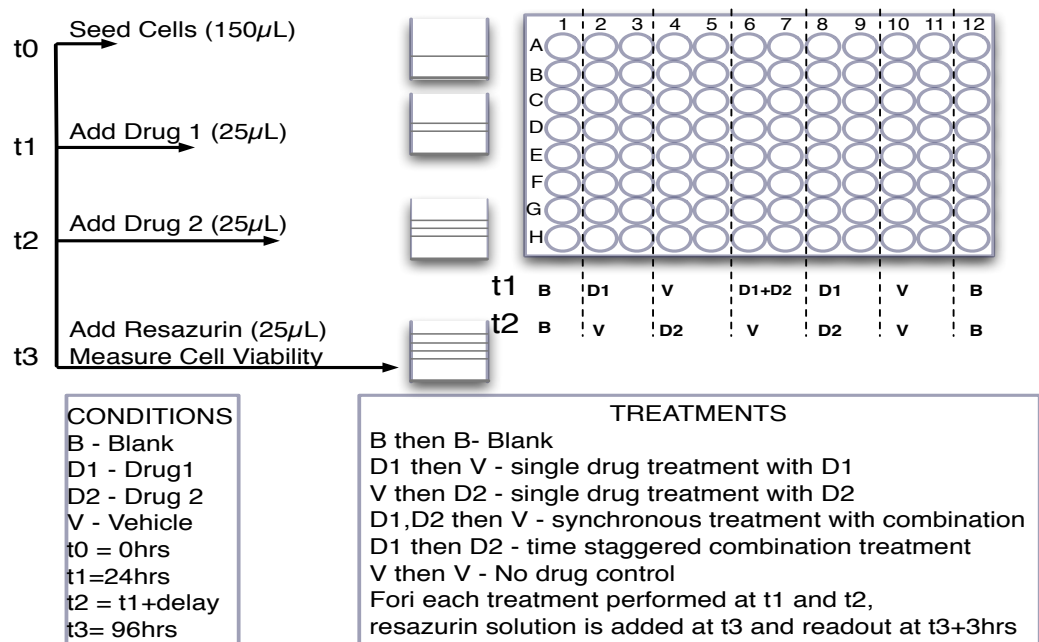

Figure 9. Experimental design of sequential drug application screen

Results

The combination of lapatinib with obatoclax was synergistic when administered with delay, with sequential treatment benefitting the latter combination in an order dependent manner. As the combination was also more effective than the oth-

ers we screened, we used a trypan blue exclusion based counting method to observe the effects of this combination on the cell line on cell death and growth. We observed that the drug combination was able not only to kill more cells than the individual drugs (fig 4), but also to slow the growth of the cell population (data not shown). Further, our observations of time and order dependency were confirmed by this assay
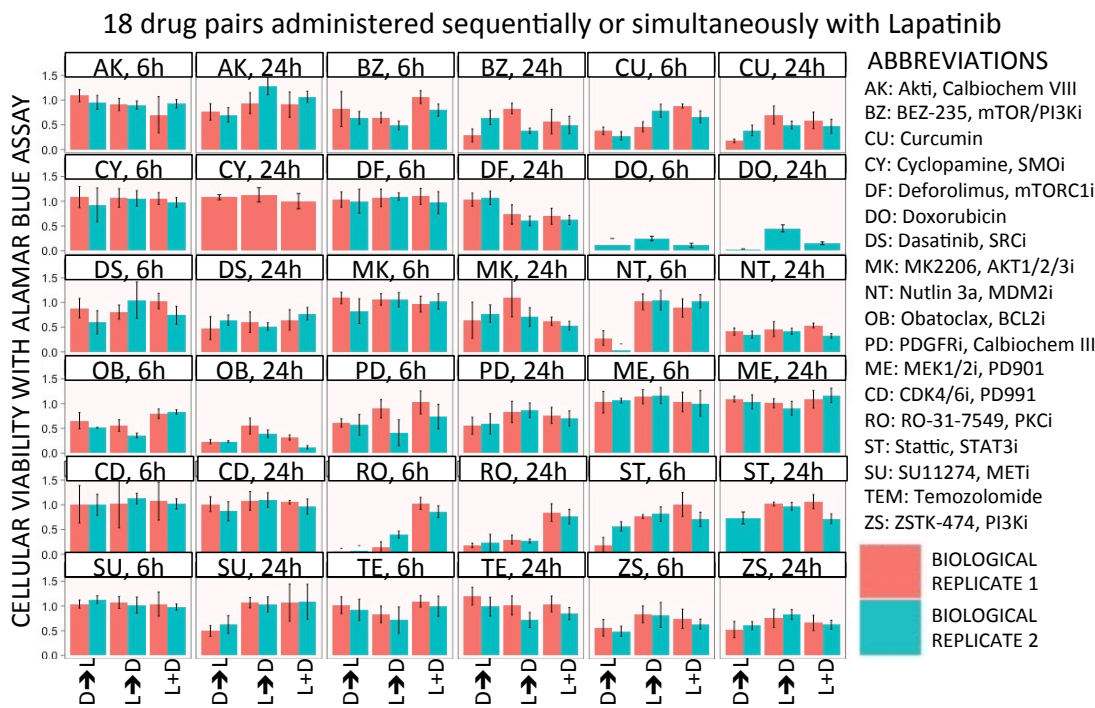

Figure 10. Fractional cellular viability resulting from simultaneous and sequential drug combinations in a screening experiment

Two other drug combinations of interest that we did not pursue further were the combinations of lapatinib with the PKC inhibitor RO-31-7549, and doxorubicin respectively. Both combinations were synergistic when administered simultaneously, as determined by our original synergy screen. In subsequent experiments using the ViCell assay, the PKC inhibitor had comparable effects on cell growth inhibition (data not shown) but continued to show enhanced cell killing when

Both Obatoclax (BCL2i) and RO-31-7549 (PKCi) cause cell death in select configurations of their combination with Lapatinib. RO-31-7549's effectiveness is greatest when administered 6h before Lapatinib whereas Obatoclax's is maximized at 24h before Lapatinib
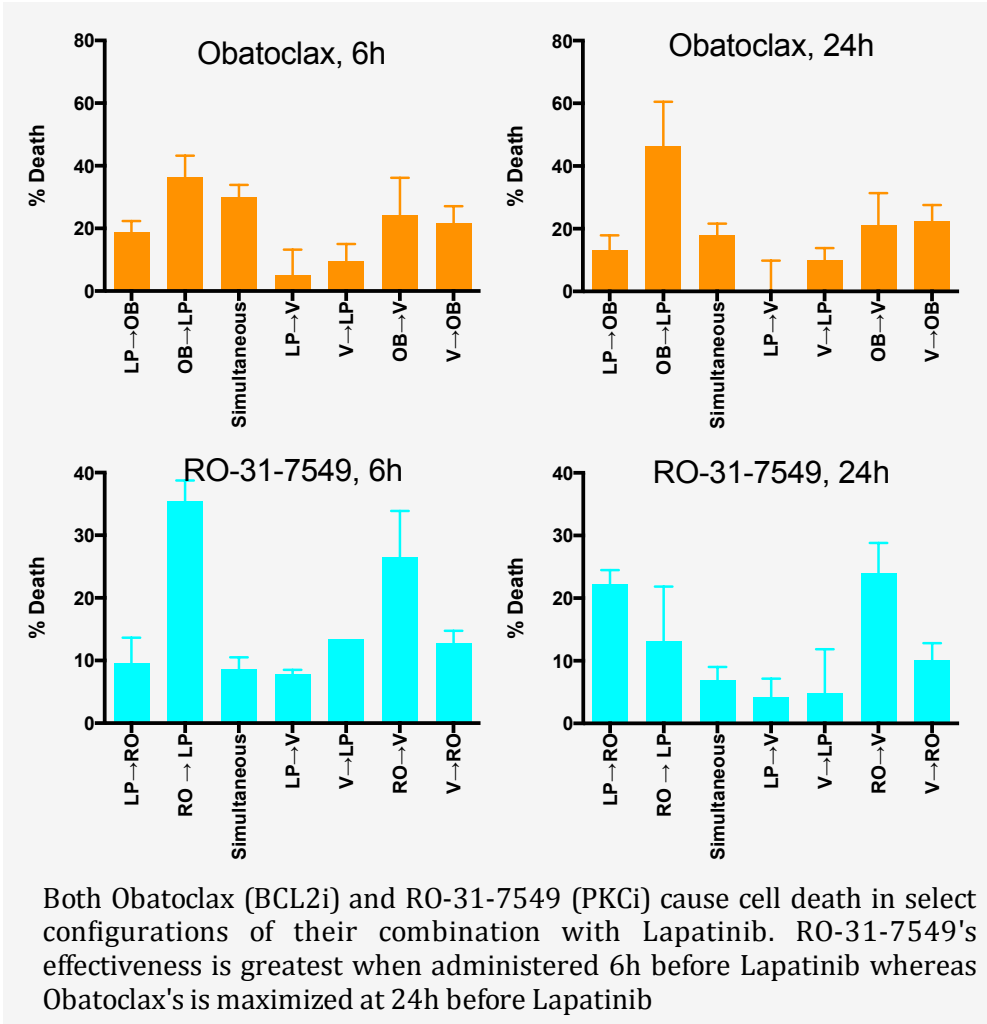
Figure 11. Fractional cell death in response to simultaneous and sequential combinations of Lapatinib with Obatoclax and RO-31-7549 respectively in tumorsphere line TS676

PKC inhibitor preceded lapatinib by 6h.

(iii) Differential effects of lapatinib and obatoclax on GBM cell lines with variable EGFR status

Rationale

To investigate whether the efficacy and synergy observed with lapatinib and obatoclax extended to other GBM tumorsphere lines, and the dependence of the observations on the EGFR status of the population, we tested the effect of these drugs on two additional cell lines – TS600, a line bearing an EGFR gain and GBM39, an EGFRvIII mutation and amplification bearing line that the lab of Dr. Frank Furnari kindly shared with us

Experiment protocol

Cells were seeded in 24 well plates, at uniform confluence near 40%. They were treated with drugs starting one day after cell seeding, and were imaged every 2h for the next 3-4 days. Per user defined settings, Incucyte ZOOM™ reported the average confluence from a total of 9 images spanning the area of the well. This choice reduced the variation arising from any cellular unevenness that might result from temperature or motion effects.

Results

(a) Pretreatment with obatoclax is beneficial in TS676 but not in TS600 or GBM39

The combination reduced the observed cellular density in both cell lines synergistically but delay was mildly beneficial in TS600 (in the condition where lapatinib preceded obatoclax) and increased rate of cell growth in GBM39. As images

taken early in the experiment occur while drugs are being added to various wells across the plate, there is frequent plate displacement and cellular motion with drug addition until the end of one day. That makes the early phase of each curve less reliable than after one day. Hence we also quantified the effect of each treatment by evaluating the slope of the growth curve in a 4 hour window centered at 3 days (fig. 5, below).
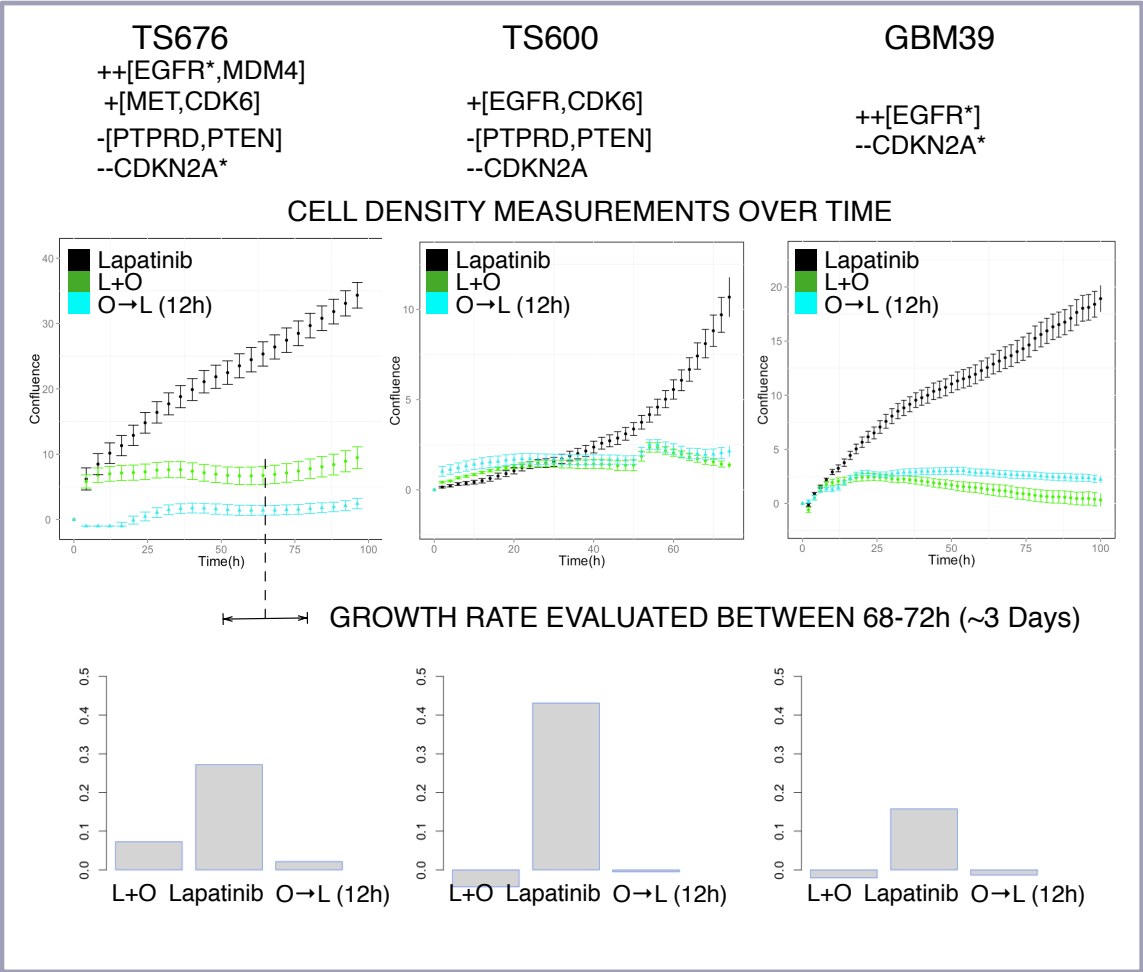

Figure 12. Pretreatment with Obatoclax before Lapatinib favors cell death in TS676

(c) Obatoclax and lapatinib cause distinct morphological changes in TS676 upon exposure to different treatment regimens

Changes in TS676 cell density and morphology over time as observed using the Incucyte ZOOM.
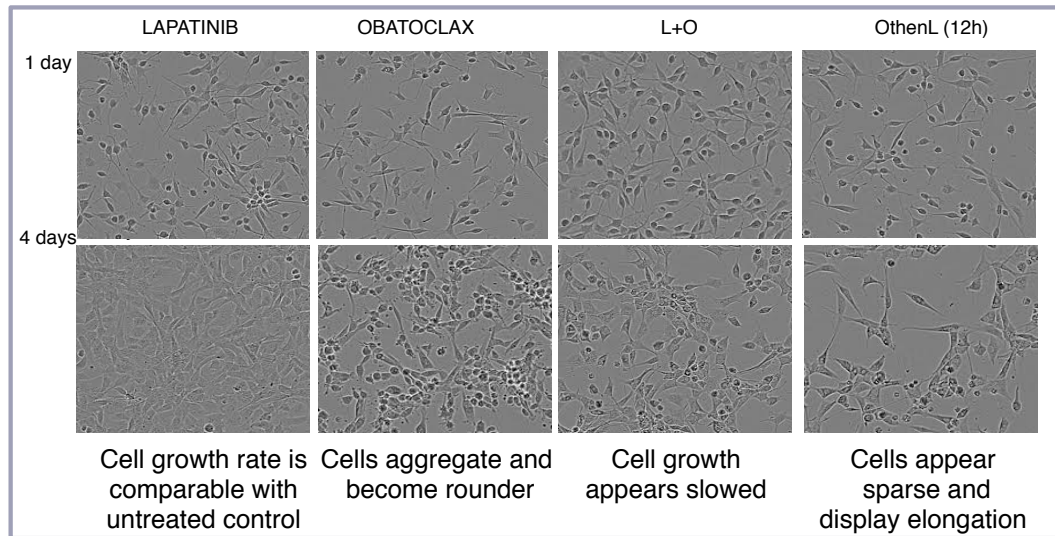
Figure 13. Changes in TS676 cell density and morphology in response to different drug treatments as observed with Incucyte ZOOM™

These qualitative observations motivate the use of addditional quantitative methods for the acquisition of a greater number of therapeutically relevant phenotypic responses from these data.

(iv) Protein response to sequential and single treatments with Western Blots reveals time dependent potentiation of pAKT by obatoclax

We next investigated the effects of these treatments on the levels of pAKT-pS473 as measured using Western Blots. We wanted to explore whether there were any obvious protein level differences between the response of these cell lines to lapa-

tinib treatment, at a protein downstream of lapatinib's target EGFR. when performed with and without obatoclax pretreatment. We observed a strong potentiation of pAKT levels with longer exposure to obatoclax in TS676 that was not mirrored by TS600. Further, this increase in pAKT persisted in TS676 that had been subjected to short pre-treatments with obatoclax, reaching maximal activity at 12h of pretreatment but then dropping when pretreated with obatoclax for 24h.

By contrast, TS600 did not show a similar lapatinib response to pAKT levels when we compared single administration of lapatinib with the obatoclax pretreatment conditions.
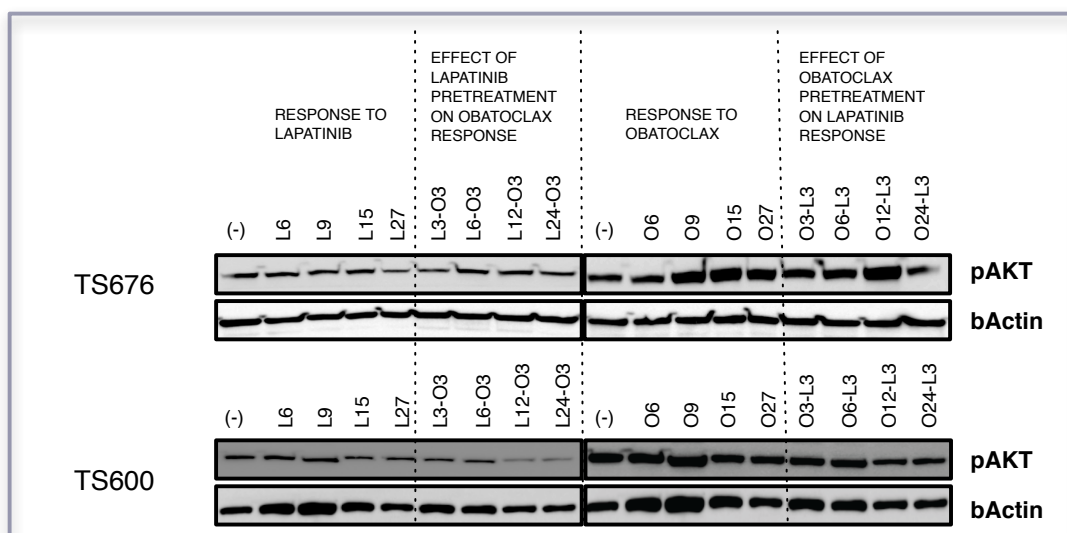

Figure 14. Protein response to sequential and single treatment with lapatinib and obatoclax in TS676 reveals time dependent potentiation of pAKT by Obatoclax

Protocol

Cells were seeded in 6 well plates at 70% confluence and treated with drugs for the times indicated. After the treatment period, cells were scraped off each well

50

over ice and the pellets obtained were lysed with a RIPA based buffer. Protein extracts were stabilized in SDS and 2-mercaptoethanol and loaded into the wells of a 4-15% western blot gel. After the proteins were run, they were transferred to a nitrocellulose membrane and imaged.

(v) Protein correlates of response to single, simultaneous and sequential treatment in TS676 and TS600.

Rationale

The behavior of pAKT in response to the treatment regimens we tested was unexpected. To our knowledge, the time dependent potentiation of pAKT by BCL2 inhibitors behavior has not yet been reported in any other cell line or system. Prior knowledge about the pathways that connect the targets of lapatinib and obatoclax indicates that RTK activation leading to the phosphorylation of AKT can inhibit apoptosis by inhibiting a family of FOXOs including FOXO3a [108, 109], proteins that transcriptionally activate diverse pro-apoptotic pathway members. In this paradigm, AKT activity can affect the level of apoptotic proteins accessible to a second drug targeting them, such as obatoclax. Further, the combination of lapatnib and obatoclax has been shown to lead to autophagic responses [110, 111] but the contribution of each drug towards the effects observed remains to be understood.

Towards explaining the effect of obatoclax on AKT mediated signaling and its effect on the observed synergy, we investigated the time dependent behavior of 46 proteins in response to the drugs administered singly, simultaneously and sequentially in both orders, with a time delay of 12h, which corresponded to the

time interval at which the observed effect of the combination was maximized when obatoclax preceded lapatinib in TS676. We selected the time points at which to capture protein profiles based on our prior experience with these lines. To enable to detection of slow and sustained changes in protein levels, we incorporated cell collection every 12 hours after treatment, up to 36 hours. Further, for each treatment applied, we collected additional samples 15 minutes and 1.5h into treatment, to observe early phosphoprotein response to these inhibitions.
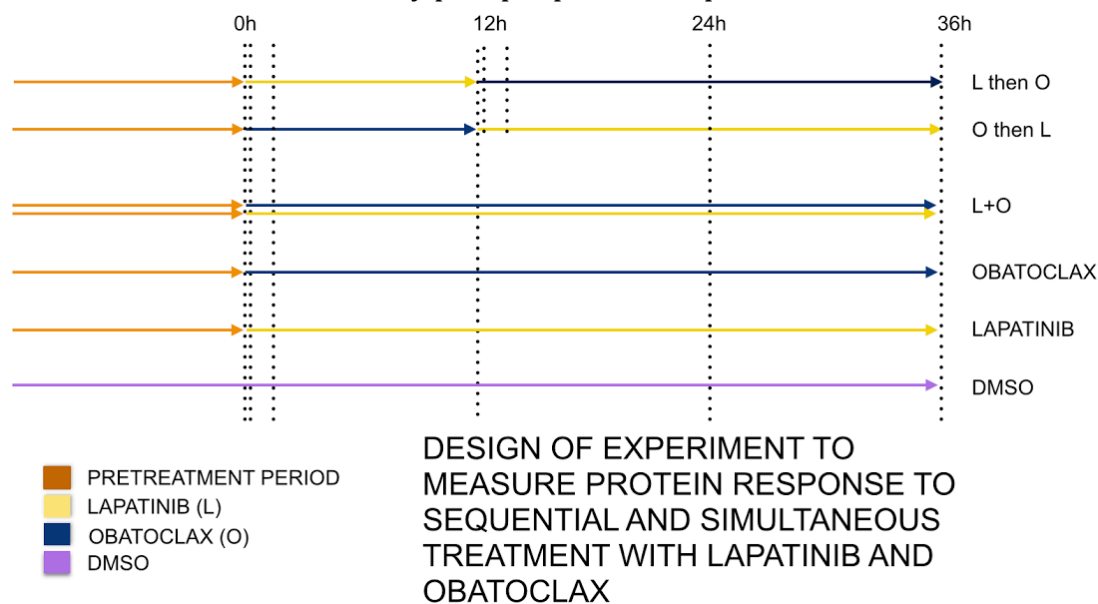
Figure 15. Design of experiment to measure protein level changes in response to sequential and simultaneous treatment with lapatinib and Obatoclax in TS676 and TS600

Protocol

To perform this experiment, we used the Zeptosens protein array system described earlier in this thesis. Samples were prepared in manner similar to that for Western Blots. Cell pellets were lysed in a Urea based buffer and robotically spotted at four dilutions and 3 biological replicates each onto the surface of Zeptosens

glass slides. The relative protein activity of each sample relative to positive control spots on each slides was quantified and reported. Examples of the time courses obtained over the conditions tested are in the figure overleaf.

Results and Discussion

The data from this experiment lead us to a few qualitative observations. The sequential treatment of T676 with obatoclax followed by lapatinib 12 hours later, which was also the most effective treatment in this cell line, displayed the highest cleaved caspase 3 levels at the end of treatment. This observation could indicate that lapatinib is able to more effectively engage the apoptosis pathway in cells whose state is altered by the action of obatoclax. In addition, the level of p38-MAPK rises in TS676, most noticeably in response to obatoclax. In inhibiting the mitochondrial apoptotic machinery, obatoclax could lead to the generation of reactive oxygen species (ROS) [112]. p38 MAPK is a stress inducible kinase that can respond to ROS and mediate both differentiation and cell death [113, 114], raising the possibility that it mediates the effects observed in treatments that include obatoclax.

Prior studies have observed the induction of autophagic phenotypes and proteins in response to the combination of drugs, as well as the inhibition of ERBB family members in response to lapatinib and its combination with obatoclax [110]. However, how the interaction of the drugs' targets and downstream effectors leads to these phenotypes remains to be understood. Further, the relationship between combination effects resulting from these drugs and the genotypes of GBM tumors and cell lines has not been studied and the effect of combined EGFR and PTEN status on the combination's ability to inhibit growth is not known. This

is particularly relevant in the context of GBM, where the amplification of EGFR with PTEN inactivation is a frequent co-occurrence. One of the reasons why the role of EGFR status on drug effects in GBM is a challenging area of study in cell-lines is that the EGFR amplicon can be lost easily over the course of passaging. The use of tumorsphere cultures in early passages, as in our work, may enhance our understanding of combination effects by retaining key alterations present in the parent tumor.

One of the open questions from our work is how delivery order and timing impacts combination effects. It is possible that by acting 12h into treatment rather than in the beginning, lapatinib could be causing the inhibition of MAPK and AKT signaling at a time when resistance mechanisms against obatoclax are being recruited. We observe that the levels of both total and phosphorylated ERK1/2 are lowered at 24h in the obatoclax before lapatinib (OèL) condition, whereas they have begun to rise after early inhibition in all conditions where lapatinib is administered early, i.e. single administration (L), simultaneous administration (L+O) and lapatinib before obatoclax (LèO). While individual observations consistent with known pathway biology can aid our understanding of the mechanism of a drug or combinations, a network view of responses to perturbation can be beneficial. A goal of network analysis would be to quantitatively relate the protein targets of a perturbation to the oncogenic phenotypes observed, through downstream effectors of each protein target. Identifying both the nodes and edges in a network that are altered in the GBM tumorsphere lines of interest, and how these are altered by drugs, could lead to an understanding of the genetic context in which the drug combinations we studied are the most effective, and subsequent cohort studies in non-human animals and clinical trials.

Future work

We have begun more detailed quantitative analyses of the data acquired. A useful method by which to identify correlations in complex multivariate data is that of partial correlations. The partial correlation between sets of variables, observed over a series of conditions, can provide insight into direct associations that drive system behavior [115]. In our data, because the protein levels observed at various points along a time course are correlated to one another, using naïve partial correlation methods that do not apply to time course data can be misleading. An effort by the lab of Dr. Korbinian Strimmer[116], to evaluate dynamical partial correlations that exist within time series data is available as the R package GeneNet. Applying this method to our data has demonstrated differences between the protein correlations observed between cell lines and between the different treatments and regimens (data not shown). Suggested next steps are generating hypotheses computationally, validating the observations using appropriate methods such as permutation tests and ranking the observations in order of their magnitude and statistical significance, and subsequently testing them in the lab. We hope that this work will help point us to the proteins that mediate the effects of obatoclax pretreatment on the efficacy of lapatinib or nominate additional targets that, in conjunction with lapatinib and obatoclax, may lead to effective treatments for EGFR amplified and PTEN deficient GBMs, which constitute a common and aggressive variant of primary glioblastoma.
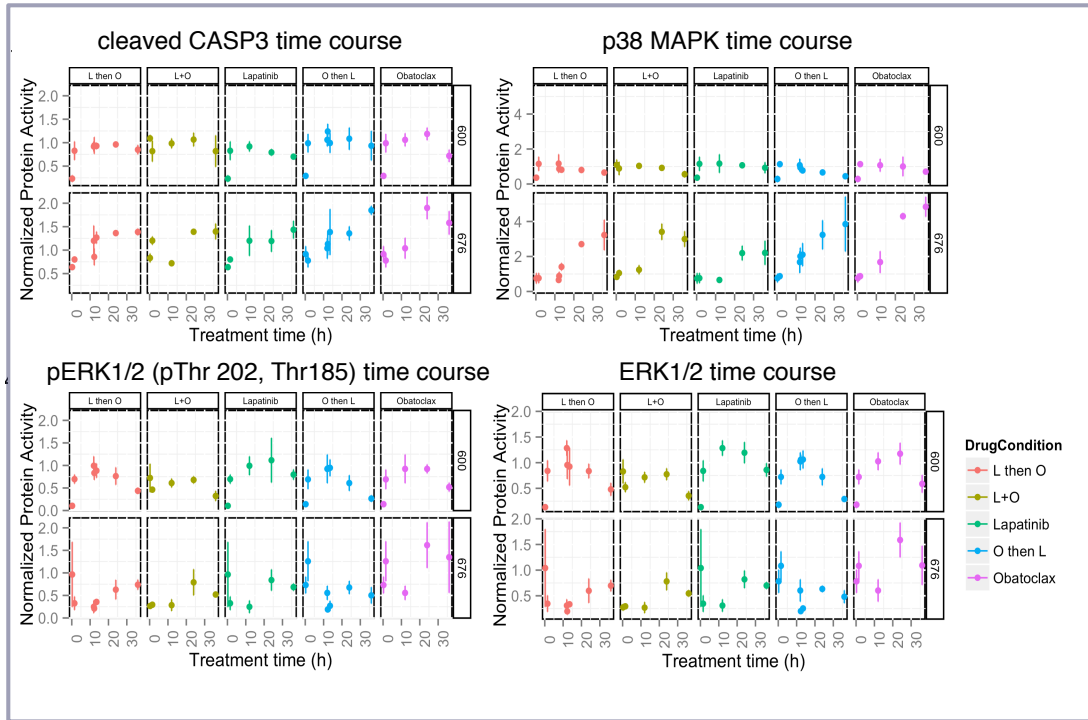
Figure 16. Time course of cleaved CASP3, p38 MAPK, and total and phosphor-ylated ERK1/2 in response to various regimens of lapatinib and/or Obatoclax in TS676 and TS600

APPENDIX
Spatial Normalization of Reverse Phase Protein array data

This work was published in PLoS One in 2014 and was joint work with other authors. I developed the method, wrote the code and all the figures. Evan Molinelli provided writing assistance. The experiments were performed by Martin Miller and Weiqing Wang, in collaboration with the listed members of the M.D. Anderson RPPA core facility and Systems Biology department. Chris Sander and Martin Miller advised me on the design of the experiments and analyses performed.

Poorvi Kaushik[1*], Evan J Molinelli[1], Martin L Miller[1], Weiqing Wang[1], Anil Korkut[1], Wenbin Liu[3], Zhenlin Ju[3], Yiling Lu[2], Gordon Mills[2], Chris Sander[1].
1 Computational Biology Center, Memorial Sloan-Kettering Cancer Center, New York, NY, USA,
2 Department of Systems Biology, The University of Texas M. D. Anderson Cancer Center, Houston, Texas, USA.
3 Division of Quantitative Sciences, The University of Texas M. D. Anderson Cancer Center, Houston, Texas, USA.

* Corresponding Author – pkaushik@cbio.mskcc.org

Abstract

Reverse phase protein arrays (RPPA) are an efficient, high-throughput, cost-effective method for the quantification of specific proteins in complex biological samples. The quality of RPPA data may be affected by various sources of error. One of these, spatial variation, is caused by uneven exposure of different parts of an RPPA slide to the reagents used in protein detection. We present a method for the determination and correction of systematic spatial variation in RPPA slides using positive control spots printed on each slide. The method uses a simple bi-linear interpolation technique to obtain a surface representing the spatial variation occurring across the dimensions of a slide. This surface is used to calculate correction factors that can normalize the relative protein concentrations of the samples on each slide. The adoption of the method results in increased agreement between technical and biological replicates of various tumor

and cell-line derived samples. Further, in data from a study of the melanoma cell-line SKMEL-133, several slides that had previously been rejected because they had a coefficient of variation (CV) greater than 15%, are rescued by reduction of CV below this threshold in each case. The method is implemented in the R statistical programing language. It is compatible with MicroVigene and SuperCurve, packages commonly used in RPPA data analysis. The method is made available, along with suggestions for implementation, at http://bitbucket.org/rppa_preprocess/rppa_preprocess/src

Introduction

In the last decade, the study of cancer biology has been accelerated by many technological advances, enabling analyses of the genome at both high resolution and throughput. This has led to the identification of mutations and biomarkers specific to various cancer types and patient subgroups. However, clinical trials of targeted therapy guided by these studies have met with less success [117, 118]. One of the reasons for this is that while the causes of cancer are genetic, they result in cellular malfunction at the level of proteins. While changes in each level may be observed discretely, they are related intimately through processes such as translation of mRNA to protein and the control of gene transcription by proteins. Further, proteins can interact with metabolites post-translationally. This increases the complexity of the proteome via the existence of multiple forms of – e.g. phosphorylated, nitrosylated and methylated – molecules that vary in function. There is hence a need for reliable and affordable methods for protein measurement, at a scale capable of complementing

today's genomics studies, so that together, they may reveal the mechanisms driving cancer.

Reverse phase protein array (RPPA) technology is a powerful technique for measuring the activities of proteins from tissue- and cell-derived lysate. It is an inexpensive, high throughput, quantitative method with low sample requirements, making it ideal for large-scale proteomic profiling studies. In RPPA, small (~μl) amounts of lysate extracted from biological samples under study are evenly spotted onto the surface of glass slides coated with an absorbent material such as nitrocellulose. A single RPPA slide of 2cm×5cm can be used to simultaneously measure the levels of a protein in thousands of samples at a time, using an automated and efficient procedure that can be scaled up to hundreds of proteins [66, 119, 120]. Each slide is probed with a primary antibody against the protein of interest, sensitive to pg-ng of protein [121], followed by a secondary antibody. A colorimetric or fluorescent signal is then generated, in proportion with the secondary antibody bound, and may be quantified to yield estimates of relative protein concentration in each sample.

RPPA design has several advantages over existing methods for protein detection. Unlike methods such as Western Blotting and 2D-Gel Electrophoresis, RPPA has high throughput and low sample requirements. While other assays such as multiplexed flow-cytometry and microsphere-based assays retain some of these advantages, they are far more expensive than RPPA and are often more labor intensive [122]. Mass spectroscopy (MS), which is another method used in large-scale protein level studies, can ana-

59

lyze the proteins in a sample using both unbiased and targeted approaches. However, current methods for MS require high sample volumes and the time required for sample analysis can be high. Reverse Phase Protein Arrays have enabled studies of protein networks implicated in different cancers [123, 124], infectious disease [125] and the responses of cells to various drugs [126-128]. However, many of the factors that make RPPA an appropriate choice for proteomics studies also introduce noise into the data. For example, the use of targeted antibodies enables the measurement of low-abundance proteins, but low antibody specificity can lead to promiscuous binding and false positives [129, 130]. Similarly, the handling of low sample volumes can lower the signal to noise ratio of the results [131]. The reliability and reproducibility of RPPA data are a key determinant of the utility of such studies. We examine one factor that contributes to noise in the RPPA data – spatial heterogeneity – and describe a method for correcting it, thereby enhancing the quality of the data.

Spatial variation in RPPA slides occurs due to unequal exposure of the slides to the experimental reagents used. This causes non-uniform signal generation, resulting in systematic variations across the area of each slide. Spatial heterogeneity is obvious when identical samples distributed over a slide produce variable signal intensities. Consequently, variance across identical samples serves as a reference with which one can measure and then correct errors arising from this heterogeneity (Fig. 1). We show that spatial differences affect the results of RPPA data obtained from diverse biological datasets. We use a simple, flexible and powerful 2D interpolation method to normalize the data, resulting in significantly enhanced data

quality as measured by improvements in reproducibility and the signal to noise ratio of the results. Also, data from antibodies that were previously unusable are rescued with the method, improving the utility of the studies performed. R code for the method is provided as a package that can be used in conjunction with MicroVigene, currently a widely used platform for the analysis of RPPA data.
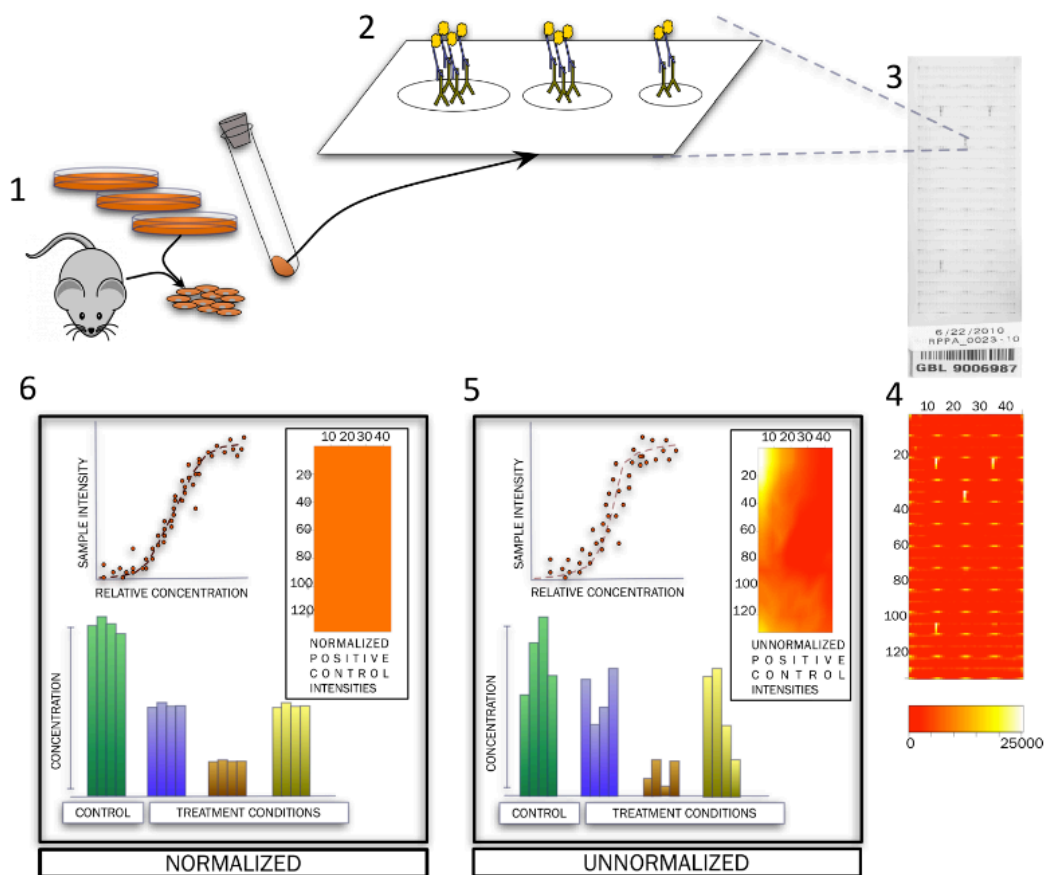
Figure 1. Steps in the acquisition and processing of RPPA data. Cells derived from different in vitro and in vivo systems are lysed and protein extracted (1). Serially diluted extracts are printed onto the surface of slides (2) where primary and secondary antibodies bind to the protein of interest and generate a signal proportionate to the amount of protein in each sample. Each slide can accommodate 5808 printed spots, for different numbers of total samples depending on the layout and number of dilutions used (3). Readouts obtained are translated to sample intensities after scanning and processing of the slides

(4). Intensities of positive control spots (horizontal yellow spots in (4)), which are technical replicates of each other, may be used to evaluate and correct spatial variation observed in each slide. Spatial correction of data can improve data quality resulting in better estimates of relative protein concentration and improved agreement between inter- and intra-slide replicates from various experiments.

Materials and Methods
Data sets analyzed using normalization routine
RPPA data for this study were obtained from slides printed with various human cell-line and tumor derived samples and probed with antibodies specific to proteins relevant to the study. The details of the method are provided in the results. We tested this method on the following data sets.

1) **Set A - Quality control samples**. This dataset was comprised of 16 slides, each identically printed with sample and then queried with a single primary antibody. The samples in these slides were obtained from a quality control study performed in the M.D. Anderson Cancer Center RPPA core-facility and a list of the antibodies used is provided in supplementary table S2.

2) **Set B - Human melanoma cell line-derived samples**. This data set was obtained from experiments performed in-house in the Sloan Kettering Institute. The melanoma cell line SKMEL-133, a [V600E]BRAF/PTEN null mutant cell line kindly gifted to us by Dr. David Solit, MSKCC [132], was perturbed with 10 small molecule inhibitors (supplementary table S1) targeting specific kinases that control cell death and proliferation. Cells were treated with each drug individually as well as with all pairwise combinations of the drugs. Three biological replicates of each experimental condition were generated, constituting approximately 300 samples that were measured with RPPA. Cell lysate from each sample was spotted onto slides and probed using 159 antibodies (supplementary table S2) to measure the quantities of clinically relevant proteins or phospho-proteins in those samples. Several of the slides were probed with the same antibody 2-3

times, resulting in a total of 238 slides and 53 antibodies with replicate slides.

3) **Set C – Miscellaneous anonymized samples**. A data set comprised of 30 slides from cell-line data processed at the M.D. Anderson Cancer Center.

Preparation, layout, printing and quantification of lysate array samples

Homogenized cell pellets consisting of cellular proteins are derived from cells grown *in-vitro* or from tissue samples *in-vivo*. Samples are lysed and the protein extract obtained is diluted based on the design of each experiment. In the slides comprising the data sets in this study, each sample undergoes a ½ serial dilution four times, leading to a total of 5 concentrations per sample. These initial serial dilutions are performed manually. Diluted samples are then robotically spotted onto the surface of slides coated with nitrocellulose. In our experimental design, each sample and positive control is printed in five dilutions. The slides are laid out as grids of 132×44 spots, comprised of 48 subgrids containing 121 spots each. Thus, each subgrid accommodates 22 samples and 2 positive control samples, in 5 dilutions each. A subgrid is also printed with a single buffer spot that serves as a negative or background control. Each slide thus accommodates 1056 serially diluted samples and 96 positive control samples (with 5 dilutions per sample), and an additional 48 negative control spots (Fig. 2). The positive control spots, are printed at fixed intervals across the length and breadth of each slide, and are technical replicates of each other, obtained from a single batch of standard mixed cell lysate [133]. Since the

controls are designed to contain sufficient amount of each of the proteins in the antibody panel for reliable detection, similar levels of the concerned protein should also be detected in experimental samples when the appropriate dilution of antibody is used. The negative control spots consist of buffer containing no protein and are hence informative of the level of background signal generated.
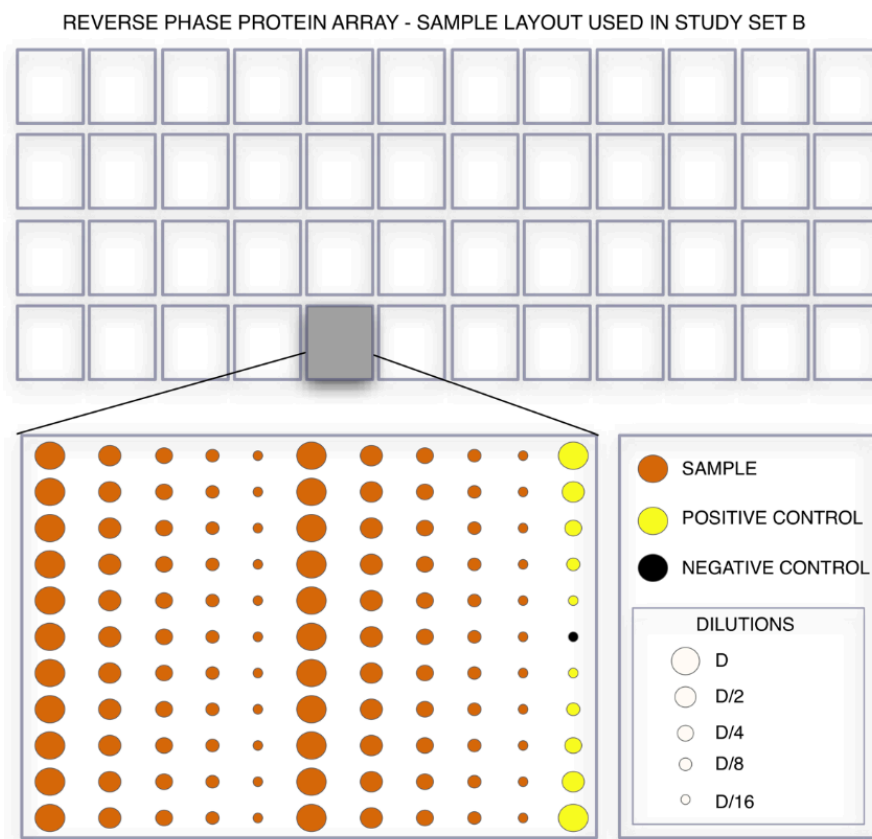

Figure 2. In the experimental design we use for the analysis of the samples in sets A and B, lysate is spotted in 96 arrays consisting of 22 samples, two positive controls and one buffer spot each. Each of the samples and the positive controls is printed in five 1:2 serial dilutions each.

Protein in each sample is quantified by washing the slide with a solution of primary antibody followed by secondary antibody. The biotinylated secondary antibody interacts with a streptavidin bound peroxidase to catalyze the deposition of a biotinylated brown tyramide compound on the surface of the spot. The intensity of the colored signal thus generated is proportional to the amount of secondary antibody and protein bound to the slide. Signal intensities obtained by scanning images of the slides were quantified by MicroVigene software [134]. These are then translated into relative protein concentrations using an R package called SuperCurve [135]. SuperCurve estimates the concentrations of all the samples on a slide with respect to one another. The estimation is based on the assumption that all the samples on a slide lie on a single dose response curve, since the hybridization kinetics of all samples have similar chemistry. The curve thus obtained may be used to obtain the relative concentration of each sample on the slide.

Assessment of data quality

The effectiveness of normalization was assessed based on the behavior of biological and technical replicates compared before and after normalization. Successful normalization should reduce noise, resulting in improved comparability of data and should bring replicates closer to each other. We define **technical replicates** as spots that are printed from lysate that was obtained from a single batch of cells in a single experiment. When printed onto a single slide, they are called intraslide replicates and when printed onto different slides, they are interslide replicates. For example, all the positive control spots belonging to a single dilution on a single slide are

intraslide technical replicates because they were obtained from a single mix of cells and subjected to dilution in a batch before the lysate was printed onto slides. **Biological replicates** are spots that are printed from cell lysate obtained from cells that were subjected to the same experimental conditions, but in separate batches. For example, in procuring dataset B, SKMEL-133 cells were grown in 3 different petri-dishes, and each was subjected to normal medium spiked with a dose of EGF ligand. They were then used to yield three separate cell pellets that when lysed and printed onto a slide, gave rise to biological replicate spots.

We expect technical and biological replicates to have different degrees of variability. Similarity of technical replicates is indicative of the reliability and uniformity of steps in the procedure such as printing, probing and scanning. On the other hand, biological replicates may vary for a number of reasons. The heterogeneity inherent to populations of cells obtained from both cell lines and tumors may make subsets of such populations behave differently when subjected to the same treatment. Several other factors could introduce biological variation, such as time to freezing and the presence of stromal and endothelial cells in tumor-derived samples, or the sample preparation method used [136-139]. Thus when technical variability is low, the differences between biological replicates can yield useful information about cellular variability in the samples studied.

To determine how spatial normalization improves the quality of RPPA data, we calculated

1. Agreement between interslide and intraslide technical replicates across 16 pairs of duplicate slides from dataset A, and 53 pairs of duplicate slides from dataset B.

2. Agreement between intra-slide biological replicates in a 238-slide melanoma cell line study.

   Agreement was evaluated with the Pearson's correlation (ρ) between corresponding spot intensities (I_A and I_B) across duplicate slides and the coefficient of variation (%CV) between replicates within-slide, where μ denotes the mean and σ the standard deviation of the spot intensities (I) or protein concentrations (P) measured.

$$\rho_{I_A, I_B} = \frac{\text{cov}(I_A, I_B)}{\sigma_{I_A} \sigma_{I_B}} = \frac{E[(I_A - \mu_{I_A})(I_B - \mu_{I_B})]}{\sigma_{I_A} \sigma_{I_B}} \quad\ldots\ldots\ldots\ldots \quad (1)$$

$$\%CV = \frac{\sigma_P \times 100}{\mu_P} \quad\ldots\ldots\ldots\ldots \quad (2)$$

Results

Bilinear interpolation of correction factors to remove spatial biases in RPPA data

The central assumption is that in the absence of spatial variance all positive controls of a given dilution should yield equal intensities. Consequently, observed variability of positive control intensities is a survey of the spatial bias on the slide. With this information, we can systematically factor out the spatial bias at any location based on neighboring positive control intensities.

We define the relationship between the measured sample intensity I(x,y) and the true intensity I′(x,y) in terms of a correction factor CF(x,y) that represents spatial variance.

$$I'(x,y) = \frac{I(x,y)}{CF(x,y)}$$

Correction factors are simply the ratio of positive control intensities PCI(x,y) to some reference intensity <PCI>.

$$CF(x,y) = \frac{PCI(x,y)}{\langle PCI \rangle}$$

Here, we choose the mean positive control intensity <PCI> to be the reference intensity. CF values above 1 indicate regions on the slide where there is a bias towards larger intensities. CF values below 1 indicate regions on the slide where there is a spatial bias towards smaller intensities.

However, these correction factors are not directly calculable at sample locations precisely because those locations do not contain positive controls. To compensate for this missing information, we use interpolation to approximate *pseudo*-positive control intensities at the sample locations.

Interpolation is the calculation to approximate the value of a function f(x,y) at specific locations (x,y) given fixed knots or measured function values at neighboring locations f(xc, yc) and is analogous to "Connect the Dots". Linear interpolation means we connect the dots with lines. The points lying on the lines between the dots are the interpolated values, and the dots themselves are fixed knots or anchor points. The interpolated

values are approximations inferred based on nearest neighbor data. In this case, we will use the measured positive control intensities to interpolate or approximate pseudo-positive control intensities at all locations on the slide.

Consider a location (x,y) that lies between four measured positive control spots with corresponding intensities *PCI(x$_a$,y$_a$)*, *PCI(x$_a$,y$_b$)*, *PCI(x$_b$,y$_a$)*, *PC(x$_b$,y$_b$)*.

$$PCI^*(x,y_a) = \frac{x_b - x}{x_b - x_a} PCI(x_a,y_a) + \frac{x - x_a}{x_b - x_a} PCI(x_b,y_a)$$

$$PCI^*(x,y_b) = \frac{x_b - x}{x_b - x_a} PCI(x_a,y_b) + \frac{x - x_a}{x_b - x_a} PCI(x_b,y_b)$$

$$PCI^*(x,y) = \frac{y_b - y}{y_b - y_a} PCI^*(x,y_a) + \frac{y - y_a}{y_b - y_a} PCI^*(x,y_b)$$

These are pseudo-positive control intensities (indicated by an asterisk) in that they are approximations for what a control intensity at that location would have been had it been spotted with control sample. The correction factors at these locations are calculable with simple division by the reference positive control intensity.

$$CF^*(x,y) = \frac{PCI(x,y)}{\langle PCI \rangle}$$

The bilinear interpolation calculation described above reflects only our assumptions about the smoothness of the spatial bias between measured positive control locations. It says nothing about the relationship any sample intensity has to another sample intensity. A similar correction can be applied after performing a cubic spline interpolation between the correction factors. Overall, the results of normalization using spline interpolation are similar to those with bilinear interpolation (supplementary table

S3). Hence we use the simpler of the two, bilinear interpolation, for normalization (supplementary Figure S1). Further, in the sample and control format used in our experiments, there are 96 sets of positive controls printed in 5 dilutions each. We use the median of each set as anchors for our interpolation step as this dilution is the most likely to be in the linear range of the assay for the set of antibodies used in the experiment. Users of the method are encouraged to design their experiments such that all the query samples are contained within the interpolation region of the positive controls. In our design, a portion of the slide (1/12th) does not have positive controls at its periphery and hence, each sample in this region was normalized by the closest correction factor evaluated.

Spatial normalization improves Coefficient of Variation between biological replicates.

Spatial normalization improves agreement between intraslide biological replicates in dataset B and 'rescues' previously discarded slides enabling further analysis of these proteins. Melanoma cell line samples were acquired for a large study aimed at understanding the basis of RAF inhibitor resistance in certain melanoma cell lines. Cell lysate was obtained from a melanoma cell line SKMEL-133 and subjected to various drug treatment conditions in triplicate, resulting in approximately 300 samples that were then quantified using RPPA. Agreement between the biological replicates was calculated before and after normalization. Around 10% of the slides (25/238) show increases of over 5% in agreement between biological replicates after normalization whereas only 1.2% (3/238) slides show a worsening of CV by over 5% with normalization. Despite increased

70

agreement overall, biological replicates show different degrees of improvement with spatial normalization (Fig. 3)
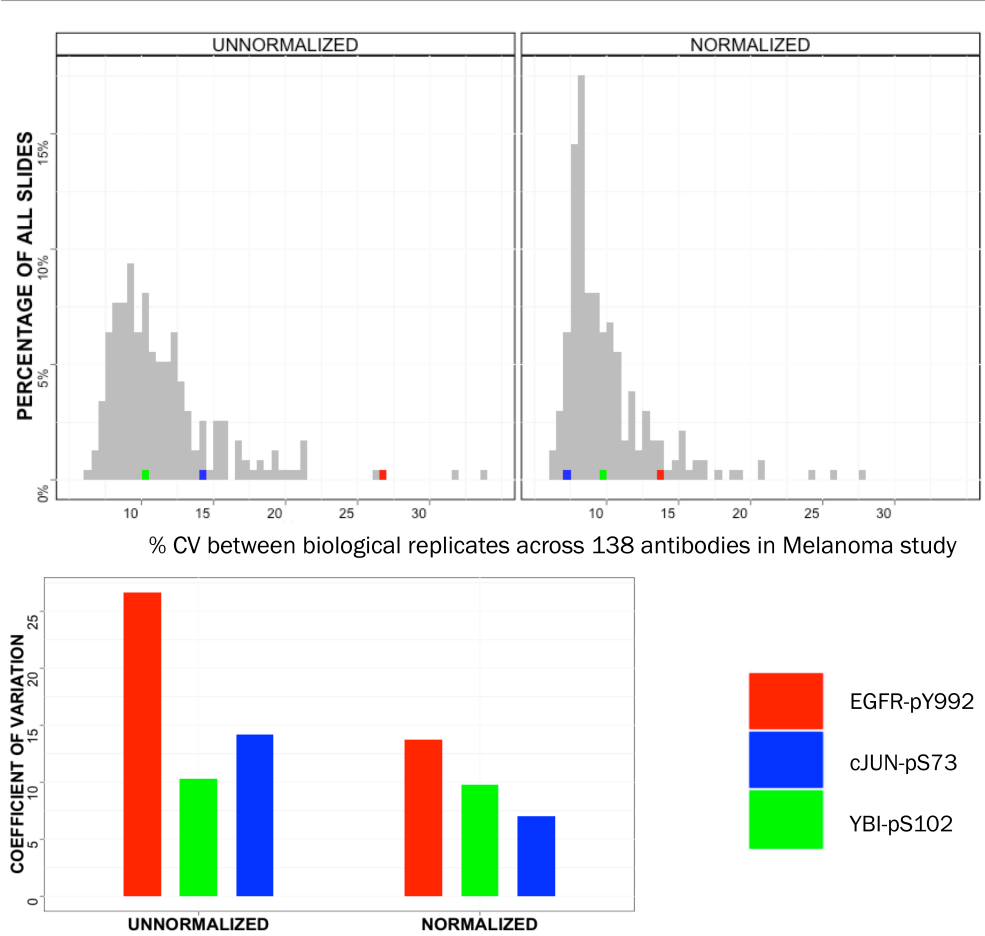

Figure 3. Coefficient of variation (%CV) of biological replicates across all antibodies before and after normalization clearly improve with normalization. The degree of improvement varies from antibody to antibody (higher for EGFR-pY992 and cJUN-pS73 than YB1-pS102) and is significant for many antibodies relevant to signaling in the melanoma cell lines studied.

The data from this study were used to train a mathematical model of melanoma biology in SKMEL-133. To maximize model accuracy, only data points with sufficient reliability were kept for model incorporation and training. Slides were selected if the average coefficient of variation (%CV) of biological replicates within each slide was seen to be less than or equal to 15%. This threshold was arbitrarily selected by the authors and is left to the discretion of the user. %CV, which is the ratio of the standard devia
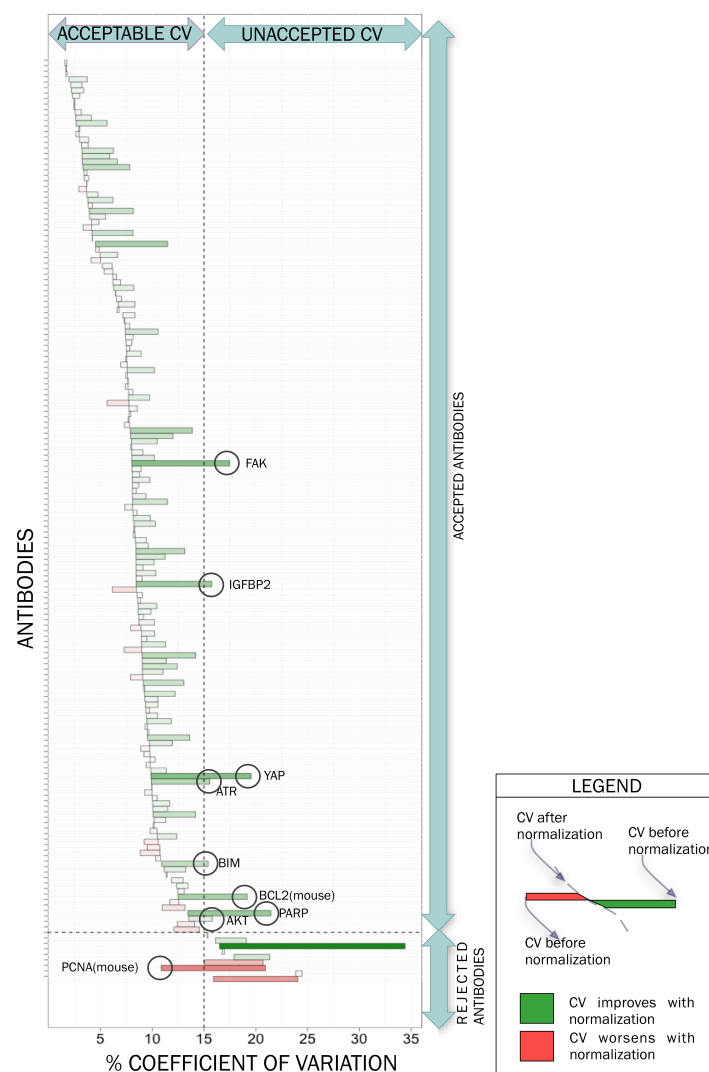

Figure 4. Spatial normalization reduces variance between biological replicates in the majority of the slides comprising a melanoma cell line study. In the study, a cutoff coefficient of variation (CV) of 15% is used to decide whether slides are retained for biological analysis. After spatial normalization, CVs in 8 slides (Caspase 9, IGFBP2, ATR, COX2,

72

FAK_pY397, BCL2(mouse), PARP, AKT) that were previously unusable drop to acceptable values. One slide - PCNA(mouse) - that had earlier been used in analysis is rejected after normalization.

tion between observations to the mean of those observations, expressed as a percentage, is a good measure of signal to noise in biological data and rises with noise in the data. A set of 168 slides was originally selected after discarding saturated and defective slides. Of the 168, when we evaluated %CV across all biological replicates in each slide, 15 slides were unusable because of %CV greater than 15%. After normalization, only 7 slides had %CV greater than 15%. The slides that were rescued by spatial normalization measured AKT, PARP, BCL2, BIM, ATR, YAP, IGFBP and FAK (Fig. 4). In certain cases, %CV appears to rise after normalization. This could reflect real noise present in the data. However, the cases where this occurs are those where %CV is significantly below the cutoff of 15% and hence this did not affect the selection of antibodies in our study. To further verify this result, we also calculated the Z'-factor [140] of each slide before and after spatial normalization. In agreement with the %CV improvements we observed in biological replicates, the per-slide Z'-factor evaluated in dataset B also improves in > 98% of the slides used in the experiment (details and calculations provided in supplementary materials, including Fig. S3).

Spatial normalization modestly improves the agreement between inter-slide replicates

To evaluate whether spatial normalization improved data quality significantly, we compared the agreement between technical and biological rep-

licates before and after normalization. We compared the Pearson's correlation of the estimated concentrations of samples printed at equivalent locations across 69 pairs of duplicate slides procured independently from sets A and B to assess interslide reproducibility. Here, duplicate slides are slides that were printed with the same samples in equivalent locations on each slide.

Many slide pairs improve in overall correlation between concentrations, with only a minority of the slide pairs showing a large such improvement. Further, slides showing a modest improvement in the behavior of interslide technical replicates with normalization often show greater improvements in concordance of biological replicates (Fig. 5 and supplementary table S4). Earlier studies using RPPA have consistently shown that such correlations evaluated between the concentrations of interslide replicates are generally high [133] but may not be the best measure of improvement in data quality after normalization.
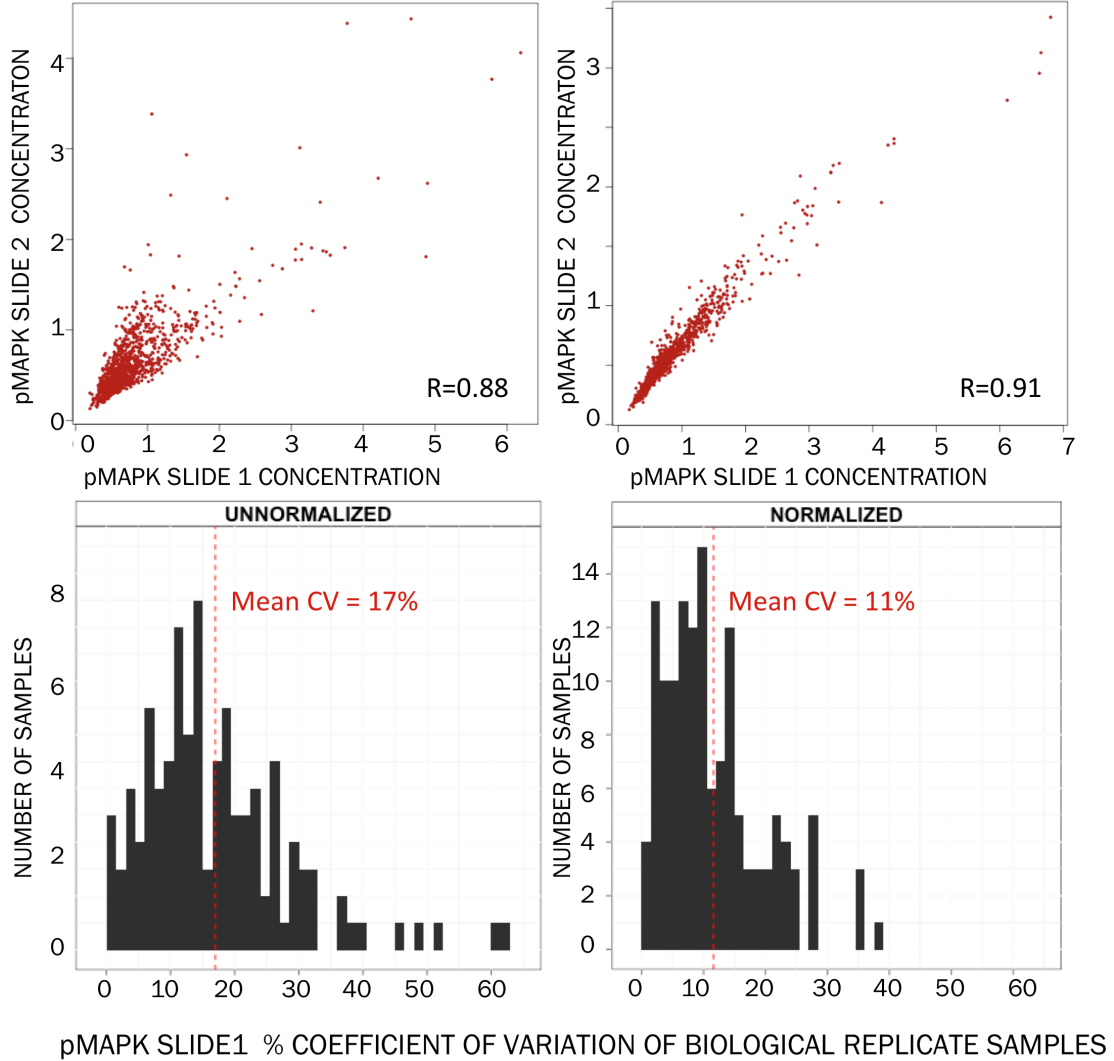
Figure 5. Correlation between concentrations of samples printed across duplicate slides increases slightly with normalization (upper panels, L→R, melanoma samples and probed with anti-pMAPK antibody). Coefficient of variation between the concentrations of biological replicates printed on one of these slides improves after normalization (lower panels, L→R).

Spatial normalization improves Intra-slide reproducibility of technical replicates

The slides evaluated for interslide reproducibility each have 480 positive controls, spotted as 96 sets of 5 dilutions each. The 96 points within a dilu-

tion are hence all technical replicates of one another. While the normalization method uses one of these sets, the median set, as anchor points for evaluating spatial variation and correction factors, we can use the remaining dilutions of the positive controls to measure %CV between each set before and after normalization. Doing this showed significant improvements in agreement between each such set of technical replicates, across most antibodies used. (Fig. 6) In the melanoma data-set, agreement between technical replicates showed an average improvement of 4%, with %CV falling from 12% to 8%, after normalization across slides probed with different antibodies. Further, 16 out of the 168 antibodies showed improvements of 10% or above in the coefficient of variation between technical replicates.
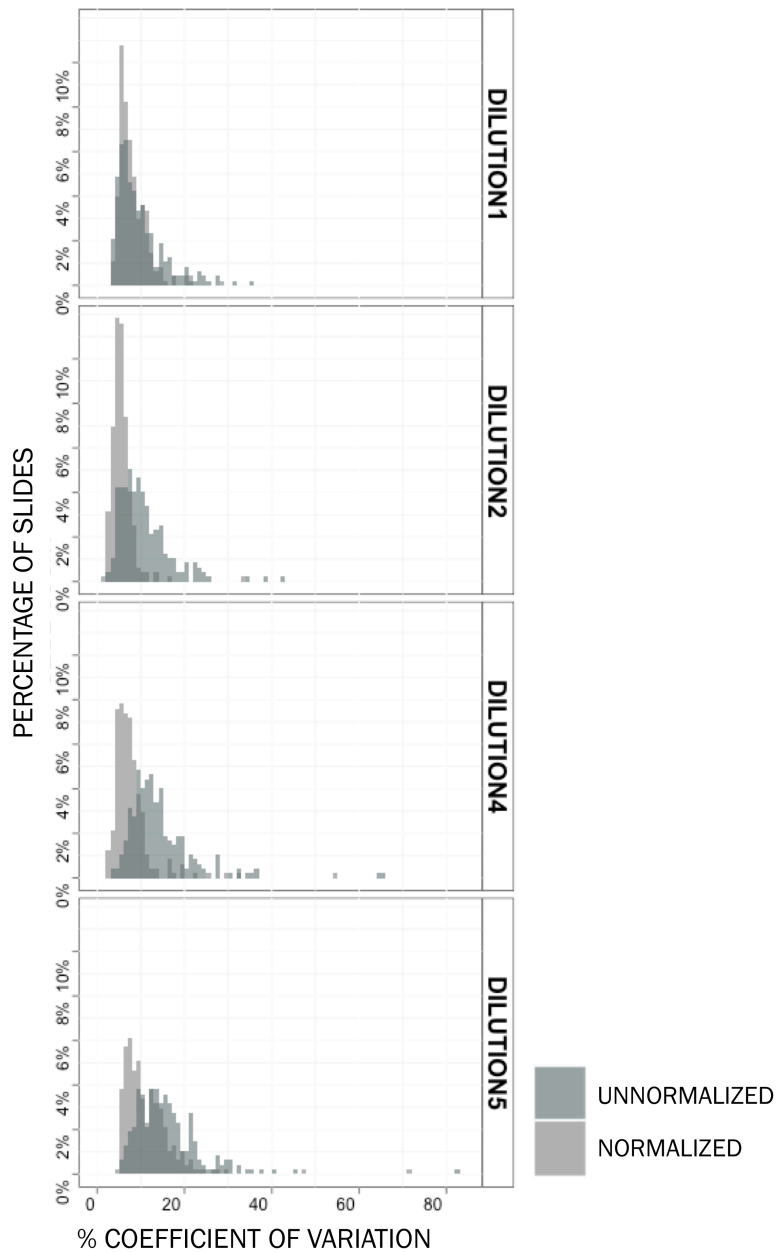
Figure 6. Coefficient of variation between intensities of intraslide technical replicates in dataset B decreases significantly with normalization. One out of 5 dilutions of positive controls is used for spatial normalization. The correlation of the remaining positive controls, which are technical replicates within each dilution, is observed after normalization. Correlations increase with normalization for each of the observed dilutions.

Discussion

RPPA is one of two main techniques used in large-scale proteomics studies today – array based techniques and mass spectrometry. High-throughput, low sample requirement and high sensitivity make it a promising technol-

ogy with which to examine protein networks in a variety of systems including cell lines and tissue samples. However, some of the features that make RPPA an appropriate choice for several kinds of proteomics studies, such as antibody-based detection, where antibodies have may different target-affinities and variable specificities, also add noise to the data it generates. Hence noise reduction and data normalization are essential for the successful application of RPPA. Our normalization technique evaluates one source of noise in RPPA data – spatial variation – and uses the measured variation to correct the data leading to increased reproducibility between duplicates in various studies. The method also makes the data from previously discarded, noisy slides usable in analysis, potentially expanding the scope of the biological questions that a set of RPPA experiments may address.

Among the genomics platforms, such as DNA microarrays, standards for experimental design and analysis have greatly improved the quality of those data and the scope of the studies that they enable [141-144]. This has lead to collaborative efforts such as the TCGA that have significantly enhanced our understanding of various cancers [1]. Among the protein activity measurement platforms, there are fewer methods that similarly address data quality. One such method [145], in which control samples are used to normalize for spatial and scaling errors in RPPA data successfully reduces intra-array replicate CV by up to 70%. However these improvements were the result of printing of as many control samples as each slide contained query samples and is hence expensive. Further, the published method was only applicable to a specified sample layout. Our method cor-

78

rects a significant and systematic source of bias in RPPA data effectively reducing error in sample sets normalized with relatively few controls. Among the melanoma data we corrected, for instance, fewer than 2% of the samples were used to normalize a total of 5808 samples. Further, the method is flexible, allowing the user to correct for spatial biases in a variety of formats containing identical control samples that contain a level of the protein of interest that is within the linear detection range of the assay used. Others in the research community have similar goals and improved standardization of analysis methods will help realize the potential of RPPA in, e.g., characterizing the signaling response to drug treatment or in training mathematical models of biological systems.

As this manuscript was completed, two other alternative methods for spatial normalization of RPPA data were published [146, 147]. The first, by Troncale et al., uses a non-parametric model that takes into account every sample's Row and Column location while fitting the obtained intensities to relative protein expressions, thus adjusting for spatial effects along with other sources of variation addressed by the paper, such as background and total protein deposited at each spot. The method of Neeley et al. is similar in ideology to ours, in that it uses the variation observed between identical controls printed at various locations on each array to normalize for spatial effects. The correction is model based, and is specific to an array format that is commonly used in the community. While a systematic comparison of existing methods would help a user to select the method best suited to their experiment and data, this is beyond the scope of our current work. We compare the changes in reproducibility of data observed

using our method with Neeley et al across the antibodies in the melanoma dataset. These results are provided in the supplementary materials (supplementary Figure S2). More extensive comparisons of the existing methods may aid in the selection of a set of standard methods for data normalization, or an improved understanding of what quantification and normalization methods work the best for different types of experiments. This would be beneficial to the RPPA community, where comparisons of experimental results are currently confounded by a lack of standardization.

A metric frequently used to assess data quality in RPPA is interslide and intraslide correlation between spot intensities of technical replicate spots [133]. While this gives us some confidence about the reliability of the results, it may not be an adequate measure of reproducibility. Since RPPA has a low dynamic range as compared to some other proteomics methods, this range is often expanded by printing multiple dilutions of each sample on the surface of a single slide. The dilutions of a sample may be widely separated in intensity, and correlations measured across all spot intensities on a slide may be biased by the range of intensities spanned by each slide (Fig. 7). When evaluating interslide correlations, we attempt to reduce this bias by comparing relative protein concentrations rather than intensities. Nonetheless, measures of intraslide technical and biological replicate equality can be more informative of data quality than Pearson's correlation. Other metrics of data quality, such as the Z'factor [140] and a Welch's t-statistic [148] to evaluate the mean difference between the positive and negative controls before and after normalization also showed im-

provements from normalization for the vast majority of samples. (supplementary figures S3 and S4).

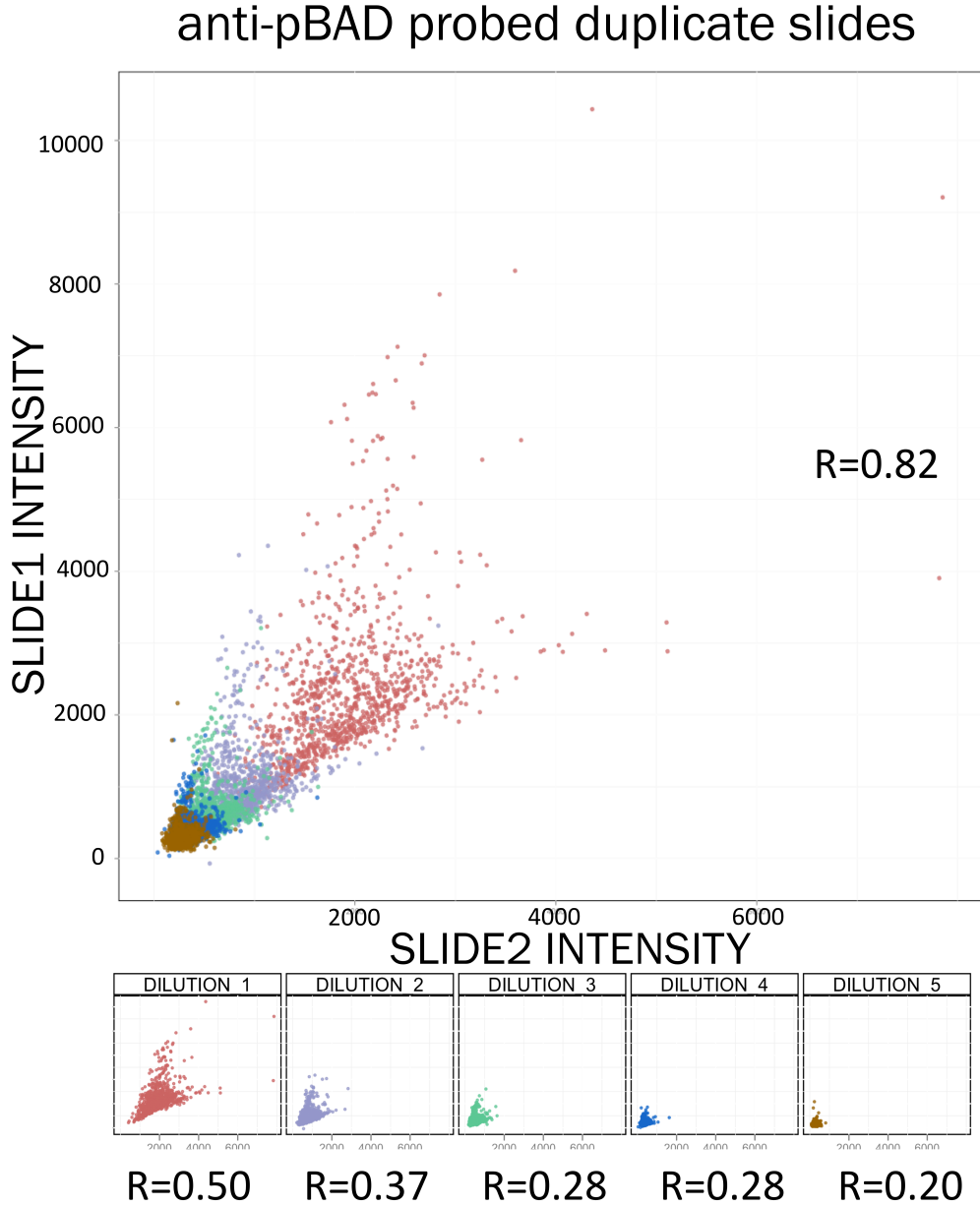Figure 7. Correlation calculations performed using intensities of all spots printed onto duplicate slides may be a misleading measure of reproducibility because of experimental design that uses multiple dilutions to evaluate sample concentrations. In the case of two identical slides probed with anti-pBAD antibody, overall correlation coefficient R=0.82 whereas correlations of the individual dilutions are lower.

The spatial normalization technique we implemented not only significantly decreased coefficient of variation improved agreement between biological and technical replicates within slides, but also made it possible to analyze the data from many slides that were previously unusable because of high variation. A particular example is our use of the antibody for PARP-1 in a study of melanoma samples subjected to various treatment conditions, where the %CV between biological replicates decreased from 21% to 13%, enabling more reliable use in the study after normalization. Poly (ADP ribose) polymerase (PARP) proteins (PARP-1 and PARP-2) play a critical role in controlling necrosis and apoptotic cell death. These PARP proteins are located inside the nucleus and take part in DNA-repair in response to DNA breaks and facilitate transcription, replication and DNA base excision repair [149]. PARP inhibitors (Olaporib, iniparib and veliparib) are undergoing clinical trials in BRCA mutated ovarian and breast cancer patients [150]. Furthermore, PARP-1 has been linked to altered control of p53-mediated DNA response and NFKappa-B response [151]. Consequently, accurate quantification of cleaved PARP-1 could be critical in understanding the complex signaling mechanisms involving PARP-inhibition as well as perturbations involving BRCA1 and BRCA2.

Other proteins similarly rescued in this and other studies could expand the scope of the biological problems addressed by RPPA. One context in which spatial normalization could be very relevant is in the analysis of tumor samples using RPPA, that due to requirements of throughput, cost and limited availability of patient material, are often unable to have sam-

ple replicates within slides. One such effort, belonging to the umbrella of TCGA projects, measures and compares protein abundance data across various tumors. In cases such as this, spatial variation alone could cause the appearance of differences that may bias the results. Hence it is very important that these data be appropriately normalized before use and analysis in other projects R code for our spatial normalization method can be used in conjunction with MicroVigene and SuperCurve. It is flexible and may be adapted to several different kinds of experimental designs, with the user specifying the locations of positive controls or other identical samples to be used as reference points for normalization.

Our method is one of several early efforts for the standardization and quality control of RPPA data. As data acquisition methods improve and RPPA moves into more widespread use, we advocate the adoption of common standards for the evaluation and correction, where possible, of systematic errors in RPPA data as well as in the analysis of these data to enable larger, multi-center studies and improve comparability across individual studies.

REFERENCES

1.	*Comprehensive genomic characterization defines human glioblastoma genes and core pathways.* Nature, 2008. **455**(7216): p. 1061-8.

2.	Brennan, C.W., et al., *The somatic genomic landscape of glioblastoma.* Cell, 2013. **155**(2): p. 462-77.

3.	Verhaak, R.G., et al., *Integrated genomic analysis identifies clinically relevant subtypes of glioblastoma characterized by abnormalities in PDGFRA, IDH1, EGFR, and NF1.* Cancer Cell, 2010. **17**(1): p. 98-110.

4.	Brennan, C., et al., *Glioblastoma subclasses can be defined by activity among signal transduction pathways and associated genomic alterations.* PLoS One, 2009. **4**(11): p. e7752.

5.	Noushmehr, H., et al., *Identification of a CpG island methylator phenotype that defines a distinct subgroup of glioma.* Cancer Cell, 2010. **17**(5): p. 510-22.

6.	Mellinghoff, I.K., et al., *Molecular determinants of the response of glioblastomas to EGFR kinase inhibitors.* N Engl J Med, 2005. **353**(19): p. 2012-24.

7.	Vivanco, I., et al., *Differential sensitivity of glioma- versus lung cancer-specific EGFR mutations to EGFR kinase inhibitors.* Cancer Discov, 2012. **2**(5): p. 458-71.

8.	Szerlip, N.J., et al., *Intratumoral heterogeneity of receptor tyrosine kinases EGFR and PDGFRA amplification in glioblastoma defines subpopulations with distinct growth factor response.* Proc Natl Acad Sci U S A, 2012. **109**(8): p. 3041-6.

9.	Snuderl, M., et al., *Mosaic amplification of multiple receptor tyrosine kinase genes in glioblastoma.* Cancer Cell, 2011. **20**(6): p. 810-7.

10. Hegi, M.E., et al., *Pathway analysis of glioblastoma tissue after preoperative treatment with the EGFR tyrosine kinase inhibitor gefitinib--a phase II trial.* Mol Cancer Ther, 2011. **10**(6): p. 1102-12.

11. Agarwal, S., et al., *Function of the blood-brain barrier and restriction of drug delivery to invasive glioma cells: findings in an orthotopic rat xenograft model of glioma.* Drug Metab Dispos, 2013. **41**(1): p. 33-9.

12. Agarwal, S., et al., *Active efflux of Dasatinib from the brain limits efficacy against murine glioblastoma: broad implications for the clinical use of molecularly targeted agents.* Mol Cancer Ther, 2012. **11**(10): p. 2183-92.

13. Nathanson, D.A., et al., *Targeted therapy resistance mediated by dynamic regulation of extrachromosomal mutant EGFR DNA.* Science, 2014. **343**(6166): p. 72-6.

14. Lee, M.J., et al., *Sequential application of anticancer drugs enhances cell death by rewiring apoptotic signaling networks.* Cell, 2012. **149**(4): p. 780-94.

15. Goldman, A., et al., *Temporally sequenced anticancer drugs overcome adaptive resistance by targeting a vulnerable chemotherapy-induced phenotypic transition.* Nat Commun, 2015. **6**: p. 6139.

16. Ren, T., et al., *Sequential treatment with AT-101 enhances cisplatin chemosensitivity in human non-small cell lung cancer cells through inhibition of apurinic/apyrimidinic endonuclease 1-activated IL-6/STAT3 signaling pathway.* Drug Des Devel Ther, 2014. **8**: p. 2517-29.

17. Kaushik, P., et al., *Spatial normalization of reverse phase protein array data.* PLoS One, 2014. **9**(12): p. e97213.

18. Smith, J.S. and R.B. Jenkins, *Genetic alterations in adult diffuse glioma: occurrence, significance, and prognostic implications.* Front Biosci, 2000. **5**: p. D213-31.

19.   Brat, D.J., et al., *Comprehensive, Integrative Genomic Analysis of Diffuse Lower-Grade Gliomas.* N Engl J Med, 2015. **372**(26): p. 2481-98.

20.   Li, A., et al., *Unsupervised analysis of transcriptomic profiles reveals six glioma subtypes.* Cancer Res, 2009. **69**(5): p. 2091-9.

21.   Vitucci, M., D.N. Hayes, and C.R. Miller, *Gene expression profiling of gliomas: merging genomic and histopathological classification for personalised therapy.* Br J Cancer, 2011. **104**(4): p. 545-53.

22.   Sturm, D., et al., *Hotspot mutations in H3F3A and IDH1 define distinct epigenetic and biological subgroups of glioblastoma.* Cancer Cell, 2012. **22**(4): p. 425-37.

23.   Brennan, C., *Genomic profiles of glioma.* Curr Neurol Neurosci Rep, 2011. **11**(3): p. 291-7.

24.   Maher, E.A., et al., *Malignant glioma: genetics and biology of a grave matter.* Genes Dev, 2001. **15**(11): p. 1311-33.

25.   Stamos, J., M.X. Sliwkowski, and C. Eigenbrot, *Structure of the epidermal growth factor receptor kinase domain alone and in complex with a 4-anilinoquinazoline inhibitor.* J Biol Chem, 2002. **277**(48): p. 46265-72.

26.   Yun, C.H., et al., *The T790M mutation in EGFR kinase causes drug resistance by increasing the affinity for ATP.* Proc Natl Acad Sci U S A, 2008. **105**(6): p. 2070-5.

27.   Filosto, S., et al., *EGF receptor exposed to oxidative stress acquires abnormal phosphorylation and aberrant activated conformation that impairs canonical dimerization.* PLoS One, 2011. **6**(8): p. e23240.

28.   Paulsen, C.E., et al., *Peroxide-dependent sulfenylation of the EGFR catalytic site enhances kinase activity.* Nat Chem Biol, 2012. **8**(1): p. 57-64.

29.   Akhavan, D., et al., *De-repression of PDGFRbeta transcription promotes acquired resistance to EGFR tyrosine kinase inhibitors in glioblastoma patients.* Cancer Discov, 2013. **3**(5): p. 534-47.

30.   Stommel, J.M., et al., *Coactivation of receptor tyrosine kinases affects the response of tumor cells to targeted therapies.* Science, 2007. **318**(5848): p. 287-90.

31.   Solit, D.B., et al., *BRAF mutation predicts sensitivity to MEK inhibition.* Nature, 2006. **439**(7074): p. 358-62.

32.   Wagle, N., et al., *MAP kinase pathway alterations in BRAF-mutant melanoma patients with acquired resistance to combined RAF/MEK inhibition.* Cancer Discov, 2014. **4**(1): p. 61-8.

33.   Landau, D.A., et al., *Evolution and impact of subclonal mutations in chronic lymphocytic leukemia.* Cell, 2013. **152**(4): p. 714-26.

34.   Park, J.H. and M.A. Lemmon, *Occupy EGFR.* Cancer Discov, 2012. **2**(5): p. 398-400.

35.   Olson, J.J., et al., *The role of targeted therapies in the management of progressive glioblastoma : a systematic review and evidence-based clinical practice guideline.* J Neurooncol, 2014. **118**(3): p. 557-99.

36.   da Fonseca, C.O., et al., *Efficacy of monoterpene perillyl alcohol upon survival rate of patients with recurrent glioblastoma.* J Cancer Res Clin Oncol, 2011. **137**(2): p. 287-93.

37.   Skipper, H.E., J.R. Thomson, and M. Bell, *Attempts at dual blocking of biochemical events in cancer chemotherapy.* Cancer Res, 1954. **14**(7): p. 503-7.

38.   DeVita, V.T. and P.S. Schein, *The use of drugs in combination for the treatment of cancer: rationale and results.* N Engl J Med, 1973. **288**(19): p. 998-1006.

39. Greco, F.A., et al., *Small cell lung cancer. Complete remission and improved survival.* Am J Med, 1979. **66**(4): p. 625-30.

40. Sos, M.L., et al., *Identifying genotype-dependent efficacy of single and combined PI3K- and MAPK-pathway inhibition in cancer.* Proc Natl Acad Sci U S A, 2009. **106**(43): p. 18351-6.

41. Frei, E.F.M.K.E.I., *Quadruple combination therapy (VAMP) for acute lymphocytic leukemia of childhood.* Proc Am Assoc Cancer Res, 1964. **5**(20).

42. McGranahan, N., et al., *Clonal status of actionable driver events and the timing of mutational processes in cancer evolution.* Sci Transl Med, 2015. **7**(283): p. 283ra54.

43. Yap, T.A., et al., *Drugging PI3K in cancer: refining targets and therapeutic strategies.* Curr Opin Pharmacol, 2015. **23**: p. 98-107.

44. Steuer, C.E., F.R. Khuri, and S.S. Ramalingam, *The next generation of epidermal growth factor receptor tyrosine kinase inhibitors in the treatment of lung cancer.* Cancer, 2015. **121**(8): p. E1-6.

45. Carlson, S.M. and F.M. White, *Using small molecules and chemical genetics to interrogate signaling networks.* ACS Chem Biol, 2011. **6**(1): p. 75-85.

46. Sanchez-Rivera, F.J. and T. Jacks, *Applications of the CRISPR-Cas9 system in cancer biology.* Nat Rev Cancer, 2015. **15**(7): p. 387-95.

47. Molinelli, E.J., et al., *Perturbation biology: inferring signaling networks in cellular systems.* PLoS Comput Biol, 2013. **9**(12): p. e1003290.

48. Miller, M.L., et al., *Drug synergy screen and network modeling in dedifferentiated liposarcoma identifies CDK4 and IGF1R as synergistic drug targets.* Sci Signal, 2013. **6**(294): p. ra85.

49. Korkut, A., et al., *Perturbation biology nominates upstream-downstream drug combinations in RAF inhibitor resistant melanoma cells.* Elife, 2015. **4**.

50.   Nelander, S., et al., *Models from experiments: combinatorial drug perturbations of cancer cells.* Mol Syst Biol, 2008. **4**: p. 216.

51.   Lehar, J., et al., *Combination chemical genetics.* Nat Chem Biol, 2008. **4**(11): p. 674-81.

52.   Lehar, J., et al., *Chemical combination effects predict connectivity in biological systems.* Mol Syst Biol, 2007. **3**: p. 80.

53.   Torsvik, A., et al., *U-251 revisited: genetic drift and phenotypic consequences of long-term cultures of glioblastoma cells.* Cancer Med, 2014. **3**(4): p. 812-24.

54.   Greshock, J., et al., *Cancer cell lines as genetic models of their parent histology: analyses based on array comparative genomic hybridization.* Cancer Res, 2007. **67**(8): p. 3594-600.

55.   Domcke, S., et al., *Evaluating cell lines as tumour models by comparison of genomic profiles.* Nat Commun, 2013. **4**: p. 2126.

56.   Calabrese, C., et al., *A perivascular niche for brain tumor stem cells.* Cancer Cell, 2007. **11**(1): p. 69-82.

57.   Gritti, A., et al., *Epidermal and fibroblast growth factors behave as mitogenic regulators for a single multipotent stem cell-like population from the subventricular region of the adult mouse forebrain.* J Neurosci, 1999. **19**(9): p. 3287-97.

58.   Reynolds, B.A. and S. Weiss, *Generation of neurons and astrocytes from isolated cells of the adult mammalian central nervous system.* Science, 1992. **255**(5052): p. 1707-10.

59.   Davis, B., et al., *Comparative genomic and genetic analysis of glioblastoma-derived brain tumor-initiating cells and their parent tumors.* Neuro Oncol, 2015.

60.   Lee, J., et al., *Tumor stem cells derived from glioblastomas cultured in bFGF and EGF more closely mirror the phenotype and genotype of primary tumors than do serum-cultured cell lines.* Cancer Cell, 2006. **9**(5): p. 391-403.

61.   Pollard, S.M., et al., *Glioma stem cell lines expanded in adherent culture have tumor-specific phenotypes and are suitable for chemical and genetic screens.* Cell Stem Cell, 2009. **4**(6): p. 568-80.

62.   González-Pinzón, R.H., Roy; Myrold, David D, *Measuring aerobic respiration in stream ecosystems using the resazurin-resorufin system.* Journal of Geophysical Research, 2012. **117**(G3).

63.   Pesch, K.L.S., U, *Combined assays for lactose and galactose by enzymatic reactions.* Milchw. Forsch, 1929. **8**.

64.   Jouanneau, S., et al., *Methods for assessing biochemical oxygen demand (BOD): a review.* Water Res, 2014. **49**: p. 62-82.

65.   Pawlak, M., et al., *Zeptosens' protein microarrays: a novel high performance microarray platform for low abundance protein analysis.* Proteomics, 2002. **2**(4): p. 383-93.

66.   Paweletz, C.P., et al., *Reverse phase protein microarrays which capture disease progression show activation of pro-survival pathways at the cancer invasion front.* Oncogene, 2001. **20**(16): p. 1981-9.

67.   Rudelius, M., et al., *Constitutive activation of Akt contributes to the pathogenesis and survival of mantle cell lymphoma.* Blood, 2006. **108**(5): p. 1668-76.

68.   Yang, J.Y., et al., *Integrative Protein-Based Prognostic Model for Early Stage Endometrioid Endometrial Cancer.* Clin Cancer Res, 2015.

69.   Mazumdar, T., et al., *A comprehensive evaluation of biomarkers predictive of response to PI3K inhibitors and of resistance mechanisms in head and neck squamous cell carcinoma.* Mol Cancer Ther, 2014. **13**(11): p. 2738-50.

70.   Nishizuka, S., et al., *Quantitative protein network monitoring in response to DNA damage.* J Proteome Res, 2008. **7**(2): p. 803-8.

71.   Ramalingam, S., et al., *Quantitative assessment of the p53-Mdm2 feedback loop using protein lysate microarrays.* Cancer Res, 2007. **67**(13): p. 6247-52.

72.   Nieto-Barajas, L.E., et al., *A time-series DDP for functional proteomics profiles.* Biometrics, 2012. **68**(3): p. 859-68.

73.   Danovi, D., et al., *Imaging-based chemical screens using normal and glioma-derived neural stem cells.* Biochem Soc Trans, 2010. **38**(4): p. 1067-71.

74.   Gallego, O., et al., *Efficacy of erlotinib in patients with relapsed gliobastoma multiforme who expressed EGFRVIII and PTEN determined by immunohistochemistry.* J Neurooncol, 2014. **116**(2): p. 413-9.

75.   Smith, J.S., et al., *PTEN mutation, EGFR amplification, and outcome in patients with anaplastic astrocytoma and glioblastoma multiforme.* J Natl Cancer Inst, 2001. **93**(16): p. 1246-56.

76.   Heimberger, A.B., et al., *The natural history of EGFR and EGFRvIII in glioblastoma patients.* J Transl Med, 2005. **3**: p. 38.

77.   Chou, T.C., *Drug combination studies and their synergy quantification using the Chou-Talalay method.* Cancer Res, 2010. **70**(2): p. 440-6.

78.   Loewe, S., *The problem of synergism and antagonism of combined drugs.* Arzneimittelforschung, 1953. **3**(6): p. 285-90.

79.   Fan, Q.W., et al., *EGFR phosphorylates tumor-derived EGFRvIII driving STAT3/5 and progression in glioblastoma.* Cancer Cell, 2013. **24**(4): p. 438-49.

80.   Wen, W., et al., *Synergistic anti-tumor effect of combined inhibition of EGFR and JAK/STAT3 pathways in human ovarian cancer.* Mol Cancer, 2015. **14**: p. 100.

81.   Li, R., et al., *Inhibition of STAT3 by niclosamide synergizes with erlotinib against head and neck cancer.* PLoS One, 2013. **8**(9): p. e74670.

82.   Zhong, H., et al., *Synergistic effects of concurrent blockade of PI3K and MEK pathways in pancreatic cancer preclinical models.* PLoS One, 2013. **8**(10): p. e77243.

83.   Haagensen, E.J., et al., *The synergistic interaction of MEK and PI3K inhibitors is modulated by mTOR inhibition.* Br J Cancer, 2012. **106**(8): p. 1386-94.

84.   Posch, C., et al., *Combined targeting of MEK and PI3K/mTOR effector pathways is necessary to effectively inhibit NRAS mutant melanoma in vitro and in vivo.* Proc Natl Acad Sci U S A, 2013. **110**(10): p. 4015-20.

85.   Park, H., et al., *Synergistic anticancer efficacy of MEK inhibition and dual PI3K/mTOR inhibition in castration-resistant prostate cancer.* Prostate, 2015.

86.   Miyoshi, S., et al., *Antitumor activity of MEK and PI3K inhibitors against malignant pleural mesothelioma cells in vitro and in vivo.* Int J Oncol, 2012. **41**(2): p. 449-56.

87.   Calabrese, E.J., *Cancer biology and hormesis: human tumor cell lines commonly display hormetic (biphasic) dose responses.* Crit Rev Toxicol, 2005. **35**(6): p. 463-582.

88.   Wikstrand, C.J., et al., *Cell surface localization and density of the tumor-associated variant of the epidermal growth factor receptor, EGFRvIII.* Cancer Res, 1997. **57**(18): p. 4130-40.

89.   Huang, H.S., et al., *The enhanced tumorigenic activity of a mutant epidermal growth factor receptor common in human cancers is mediated by threshold*

levels of constitutive tyrosine phosphorylation and unattenuated signaling. J Biol Chem, 1997. **272**(5): p. 2927-35.

90.   Grandal, M.V., et al., *EGFRvIII escapes down-regulation due to impaired internalization and sorting to lysosomes.* Carcinogenesis, 2007. **28**(7): p. 1408-17.

91.   Nakada, M., et al., *Mechanism of chemoresistance against tyrosine kinase inhibitors in malignant glioma.* Brain Tumor Pathol, 2014. **31**(3): p. 198-207.

92.   van den Bent, M.J., et al., *Randomized phase II trial of erlotinib versus temozolomide or carmustine in recurrent glioblastoma: EORTC brain tumor group study 26034.* J Clin Oncol, 2009. **27**(8): p. 1268-74.

93.   Yung, W.K., et al., *Safety and efficacy of erlotinib in first-relapse glioblastoma: a phase II open-label study.* Neuro Oncol, 2010. **12**(10): p. 1061-70.

94.   Fenton, T.R., et al., *Resistance to EGF receptor inhibitors in glioblastoma mediated by phosphorylation of the PTEN tumor suppressor at tyrosine 240.* Proc Natl Acad Sci U S A, 2012. **109**(35): p. 14164-9.

95.   Fan, Q.W., et al., *EGFR signals to mTOR through PKC and independently of Akt in glioma.* Sci Signal, 2009. **2**(55): p. ra4.

96.   Clark, P.A., et al., *Activation of multiple ERBB family receptors mediates glioblastoma cancer stem-like cell resistance to EGFR-targeted inhibition.* Neoplasia, 2012. **14**(5): p. 420-8.

97.   Kopetz, S., et al., *Improved survival in metastatic colorectal cancer is associated with adoption of hepatic resection and improved chemotherapy.* J Clin Oncol, 2009. **27**(22): p. 3677-83.

98.   Zhou, C., et al., *Erlotinib versus chemotherapy as first-line treatment for patients with advanced EGFR mutation-positive non-small-cell lung cancer*

(OPTIMAL, CTONG-0802): a multicentre, open-label, randomised, phase 3 study. Lancet Oncol, 2011. **12**(8): p. 735-42.

99.   Mitsudomi, T., et al., *Gefitinib versus cisplatin plus docetaxel in patients with non-small-cell lung cancer harbouring mutations of the epidermal growth factor receptor (WJTOG3405): an open label, randomised phase 3 trial.* Lancet Oncol, 2010. **11**(2): p. 121-8.

100.   Yun, C.H., et al., *Structures of lung cancer-derived EGFR mutants and inhibitor complexes: mechanism of activation and insights into differential inhibitor sensitivity.* Cancer Cell, 2007. **11**(3): p. 217-27.

101.   Wakeling, A.E., et al., *ZD1839 (Iressa): an orally active inhibitor of epidermal growth factor signaling with potential for cancer therapy.* Cancer Res, 2002. **62**(20): p. 5749-54.

102.   Pollack, V.A., et al., *Inhibition of epidermal growth factor receptor-associated tyrosine phosphorylation in human carcinomas with CP-358,774: dynamics of receptor inhibition in situ and antitumor effects in athymic mice.* J Pharmacol Exp Ther, 1999. **291**(2): p. 739-48.

103.   Litvin, O., et al., *Interferon alpha/beta Enhances the Cytotoxic Response of MEK Inhibition in Melanoma.* Mol Cell, 2015. **57**(5): p. 784-96.

104.   Pandey, A., et al., *Sequential application of a cytotoxic nanoparticle and a PI3K inhibitor enhances antitumor efficacy.* Cancer Res, 2014. **74**(3): p. 675-85.

105.   Dougherty, M.K., et al., *Regulation of Raf-1 by direct feedback phosphorylation.* Mol Cell, 2005. **17**(2): p. 215-24.

106.   Tullai, J.W., et al., *Immediate-early and delayed primary response genes are distinct in function and genomic architecture.* J Biol Chem, 2007. **282**(33): p. 23981-95.

107. Neeley, E.S., et al., *Variable slope normalization of reverse phase protein arrays.* Bioinformatics, 2009. **25**(11): p. 1384-9.

108. Zhang, X., et al., *Akt, FoxO and regulation of apoptosis.* Biochim Biophys Acta, 2011. **1813**(11): p. 1978-86.

109. Bean, G.R., et al., *PUMA and BIM are required for oncogene inactivation-induced apoptosis.* Sci Signal, 2013. **6**(268): p. ra20.

110. Cruickshanks, N., et al., *Lapatinib and obatoclax kill tumor cells through blockade of ERBB1/3/4 and through inhibition of BCL-XL and MCL-1.* Mol Pharmacol, 2012. **81**(5): p. 748-58.

111. Tang, Y., et al., *Obatoclax and lapatinib interact to induce toxic autophagy through NOXA.* Mol Pharmacol, 2012. **81**(4): p. 527-40.

112. Lagadinou, E.D., et al., *BCL-2 inhibition targets oxidative phosphorylation and selectively eradicates quiescent human leukemia stem cells.* Cell Stem Cell, 2013. **12**(3): p. 329-41.

113. Huot, J., et al., *SAPK2/p38-dependent F-actin reorganization regulates early membrane blebbing during stress-induced apoptosis.* J Cell Biol, 1998. **143**(5): p. 1361-73.

114. Lee, M.W., et al., *The involvement of reactive oxygen species (ROS) and p38 mitogen-activated protein (MAP) kinase in TRAIL/Apo2L-induced apoptosis.* FEBS Lett, 2002. **512**(1-3): p. 313-8.

115. Stein, R.R., D.S. Marks, and C. Sander, *Inferring Pairwise Interactions from Biological Data Using Maximum-Entropy Probability Models.* PLoS Comput Biol, 2015. **11**(7): p. e1004182.

116. Opgen-Rhein, R. and K. Strimmer, *From correlation to causation networks: a simple approximate learning algorithm and its application to high-dimensional plant gene expression data.* BMC Syst Biol, 2007. **1**: p. 37.

117. Kola, I. and J. Landis, *Can the pharmaceutical industry reduce attrition rates?* Nat Rev Drug Discov, 2004. **3**(8): p. 711-5.

118. DiMasi, J.A. and H.G. Grabowski, *Economics of new oncology drug development.* J Clin Oncol, 2007. **25**(2): p. 209-16.

119. Nishizuka, S., et al., *Proteomic profiling of the NCI-60 cancer cell lines using new high-density reverse-phase lysate microarrays.* Proc Natl Acad Sci U S A, 2003. **100**(24): p. 14229-34.

120. Espina, V., et al., *Reverse phase protein microarrays for theranostics and patient-tailored therapy.* Methods Mol Biol, 2008. **441**: p. 113-28.

121. Bender, C., et al., *Dynamic deterministic effects propagation networks: learning signalling pathways from longitudinal protein array data.* Bioinformatics, 2010. **26**(18): p. i596-602.

122. Terfve, C. and J. Saez-Rodriguez, *Modeling signaling networks using high-throughput phospho-proteomics.* Adv Exp Med Biol, 2012. **736**: p. 19-57.

123. Espina, V., J. Wulfkuhle, and L.A. Liotta, *Application of laser microdissection and reverse-phase protein microarrays to the molecular profiling of cancer signal pathway networks in the tissue microenvironment.* Clin Lab Med, 2009. **29**(1): p. 1-13.

124. Gulmann, C., et al., *Quantitative cell signalling analysis reveals down-regulation of MAPK pathway activation in colorectal cancer.* J Pathol, 2009. **218**(4): p. 514-9.

125. Molero, C., et al., *Addressing the effects of Salmonella internalization in host cell signaling on a reverse-phase protein array.* Proteomics, 2009. **9**(14): p. 3652-65.

126. Martiny-Baron, G., et al., *Characterization of kinase inhibitors using reverse phase protein arrays.* Methods Mol Biol, 2011. **785**: p. 79-107.

127. Lavezzari, G. and M.R. Lackner, *Monitoring phosphoproteomic response to targeted kinase inhibitors using reverse-phase protein microarrays.* Methods Mol Biol, 2011. **795**: p. 203-15.

128. Ma, Y., et al., *Predicting cancer drug response by proteomic profiling.* Clin Cancer Res, 2006. **12**(15): p. 4583-9.

129. Aoki, H., et al., *Telomere 3' overhang-specific DNA oligonucleotides induce autophagy in malignant glioma cells.* FASEB J, 2007. **21**(11): p. 2918-30.

130. Charboneau, L., et al., *Utility of reverse phase protein arrays: applications to signalling pathways and human body arrays.* Brief Funct Genomic Proteomic, 2002. **1**(3): p. 305-15.

131. Nishizuka, S.S., *Reverse-phase protein lysate microarray (RPA) for the experimental validation of quantitative protein network models.* Methods Mol Biol, 2011. **785**: p. 65-77.

132. Xing, F., et al., *Concurrent loss of the PTEN and RB1 tumor suppressors attenuates RAF dependence in melanomas harboring (V600E)BRAF.* Oncogene, 2012. **31**(4): p. 446-57.

133. Hennessy, B.T., et al., *A Technical Assessment of the Utility of Reverse Phase Protein Arrays for the Study of the Functional Proteome in Non-microdissected Human Breast Cancers.* Clin Proteomics, 2011. **6**(4): p. 129-51.

134. Liang, C., et al., *Calibration and Normalization of Protein Microarray Data*, in *IBC's 11th Annual International Congress, CHIPS To HITS 2004*. 2004: Boston.

135. Kevin Coombes, W.L., Zhenlin Ju, Shannon Neeley, Paul Roebuck, *SuperCurve*. 2012.

136. Bai, Y., et al., *Quantitative assessment shows loss of antigenic epitopes as a function of pre-analytic variables.* Lab Invest, 2011. **91**(8): p. 1253-61.

137.   Havelund, B.M., et al., *The Influence of Tissue Ischemia on Biomarker Expression in Colorectal Cancer.* Appl Immunohistochem Mol Morphol, 2012.

138.   Espina, V., et al., *A portrait of tissue phosphoprotein stability in the clinical tissue procurement process.* Mol Cell Proteomics, 2008. **7**(10): p. 1998-2018.

139.   Silvestri, A., et al., *Protein pathway biomarker analysis of human cancer reveals requirement for upfront cellular-enrichment processing.* Lab Invest, 2010. **90**(5): p. 787-96.

140.   Zhang, J.H., T.D. Chung, and K.R. Oldenburg, *A Simple Statistical Parameter for Use in Evaluation and Validation of High Throughput Screening Assays.* J Biomol Screen, 1999. **4**(2): p. 67-73.

141.   Listgarten, J., et al., *Clinically validated benchmarking of normalisation techniques for two-colour oligonucleotide spotted microarray slides.* Appl Bioinformatics, 2003. **2**(4): p. 219-28.

142.   Neuvial, P., et al., *Spatial normalization of array-CGH data.* BMC Bioinformatics, 2006. **7**: p. 264.

143.   Yang, Y.H., et al., *Normalization for cDNA microarray data: a robust composite method addressing single and multiple slide systematic variation.* Nucleic Acids Res, 2002. **30**(4): p. e15.

144.   Verdugo, R.A., et al., *Importance of randomization in microarray experimental designs with Illumina platforms.* Nucleic Acids Res, 2009. **37**(17): p. 5610-8.

145.   Anderson, T., et al., *Improved reproducibility of reverse-phase protein microarrays using array microenvironment normalization.* Proteomics, 2009. **9**(24): p. 5562-6.

146.   Neeley, E.S., K.A. Baggerly, and S.M. Kornblau, *Surface Adjustment of Reverse Phase Protein Arrays using Positive Control Spots.* Cancer Inform, 2012. **11**: p. 77-86.

147.   Troncale, S., et al., *NormaCurve: a SuperCurve-based method that simultaneously quantifies and normalizes reverse phase protein array data.* PLoS One, 2012. **7**(6): p. e38686.

148.   Welch, B.L., *The generalisation of student's problems when several different population variances are involved.* Biometrika, 1947. **34**(1-2): p. 28-35.

149.   Strosznajder, R.P., H. Jesko, and A. Zambrzycka, *Poly(ADP-ribose) polymerase: the nuclear target in signal transduction and its role in brain ischemia-reperfusion injury.* Mol Neurobiol, 2005. **31**(1-3): p. 149-67.

150.   Tutt, A., et al., *Oral poly(ADP-ribose) polymerase inhibitor olaparib in patients with BRCA1 or BRCA2 mutations and advanced breast cancer: a proof-of-concept trial.* Lancet, 2010. **376**(9737): p. 235-44.

151.   Valenzuela, M.T., et al., *PARP-1 modifies the effectiveness of p53-mediated DNA damage response.* Oncogene, 2002. **21**(7): p. 1108-16.